MASTER'S THESIS IN PHYSICAL OCEANOGRAPHY

Long-term changes in the Nordic Seas' hydrographic structure and overflow waters

Øystein M. Breiteig

June 16, 2020

GEOPHYSICAL INSTITUTE
UNIVERSITY OF BERGEN

Abstract

An extensive collection of historical hydrographic data was used to examine the hydrographic properties of the water masses in the Nordic Seas from 1950 to 2018, with particular focus on the dense overflows from the Nordic Seas. Around 1980 a warming trend commenced in the Greenland Sea. The main reason for this warming trend was most likely the cessation of deep convection there in the 1980s. From the Greenland Sea this warming trend spread to the other basins in the Nordic Seas, which started warming at a later time because of inflowing water masses originating in the Greenland Sea. As a consequence widespread structural changes in the hydrography of the Nordic Seas have taken place, in particular a deepening of isopycnals and an increase in volume of lighter water masses. The currents supplying the densest overflow waters to the Greenland-Scotland Ridge, the North Icelandic Jet to Denmark Strait and the Iceland-Faroe Slope Jet to the Faroe Bank Channel, have become warmer and more saline since the middle of the 1990s. The density of the water transported by the North Icelandic Jet increased by $(8.3 \pm 5.7) * 10^{-3}$ kg/m^3 per decade.

Acknowledgment

First I want to give a special thanks to my supervisor, Kjetil Våge, for all the helpful feedback, good advice, and guidance. It has been a pleasure to work with this exciting topic. I would also like to thank Ailin Brakstad and Stefanie Semper for the help and good advices I have received during the last year. Thanks also to the OVENS project group for interesting meetings, where I have learned a lot.

Secondly I would like to thank my family and friends for the great support on the way. A special thanks to my girlfriend, Anna, for always believing in me and encouraging me. Lastly I would like to thank all my fellow students over the years, I have really enjoyed the time together with you.

Contents

Chapter 1

Introduction

1.1 The Nordic Seas

1.1.1 Geography and bathymetry

The Nordic Seas are a collective term for the Iceland, Greenland, and Norwegian Seas (Figure 1.1). The Norwegian Sea can be divided into the Norwegian and Lofoten Basins, and together with the Greenland and Iceland Seas are referred to as the four basins in the Nordic Seas. The northern boundary between the Nordic Seas and Arctic Ocean is Fram Strait located west of Svalbard. In the south, the Greenland Scotland Ridge (GSR) separates the Nordic Seas from the North Atlantic Ocean. Along the GSR Denmark Strait is located west of Iceland, while the Faroe Bank Channel (FBC) lies south of the Faroe Islands. These are deep gaps in the ridge where cold water masses are transported at depth into the Atlantic Ocean. At Denmark Strait the sill depth is 630 m (Jónsson and Valdimarsson, 2004), while the FBC has a sill depth of 850 m (Dickson and Brown, 1994).

Jan Mayen is placed in the middle of the Nordic Seas at the intersection of the main submarine ridges separating the four relatively deep basins. The Greenland and Iceland Seas are both located in the western part of the Nordic Seas. These basins are separated by the West Jan Mayen Ridge, which extends westwards from Jan Mayen. The Kolbeinsey Ridge is the extension of the Mid-Atlantic Ridge north of Iceland. Both the Norwegian and Lofoten Basins are located in the eastern part of the Nordic Seas. The Mohn Ridge separates the Lofoten Basin from the Greenland Sea. The Jan Mayen Ridge lies between the Iceland Sea and the Norwegian Basin (Blindheim and Rey, 2004).

1.1.2 Circulation

The Atlantic Ocean supplies the Nordic Seas with warm and saline water masses. The warm Atlantic inflow into the Nordic Seas consist of the North Icelandic Irminger Current (NIIC) and the Norwegian Atlantic Current (NAC, Figure 1.1). The NIIC is a surface-intensified current (Jónsson and Valdimarsson, 2012) and flows northwards through Denmark Strait. East of Iceland the warm water flows into the Nordic Seas on both sides of the Faroe Islands (the Faroe and the Shetland Branches of the NAC). Another inflowing branch is located directly east of Iceland, which joins the Faroe Branch. Closer to Norway the current splits into two branches; one that follows the Norwegian continental slope and one that flows northwards between the Lofoten Basin and the Norwegian Basin and along the Mohn Ridge. The NAC continues northwards into the Barents Sea and the Arctic Ocean.

The NAC recirculates in Fram Strait and merges with the East Greenland Current (EGC). The EGC flows south from the Arctic Ocean with cold waters through Fram Strait and follows the Greenland continental slope all the way to Denmark Strait. Both the Jan Mayen Current and the East Icelandic Current (EIC) branch off from the EGC (Figure 1.1). Deep water flows from the Greenland Sea into the Norwegian Sea through the Jan Mayen Channel, with a sill depth at 2000 m. Shao et al. (2019) proposed that the Jan Mayen Channel is a regular and direct route for water transport between the Norwegian Sea and the Greenland Sea. There is also exchange between the Greenland Sea and the Lofoten Basin across the Mohn Ridge (Spall, 2010).

1.1.3 Water masses

Overflow water is categorized as water denser than $\sigma_\theta = 27.8$ kg/m^3 (Dickson and Brown, 1994). Atlantic Water is very warm and saline water transported by the NAC from the Atlantic Ocean. This water mass is cooled and densified along the Norwegian slope, before transported southward as Atlantic-Origin water. Atlantic-Origin waters are warmer and more saline than the Arctic-Origin waters, and mainly transported by the EGC and NAC. Arctic-Origin waters are cold and dense, and formed by open ocean convection in the Iceland and Greenland Seas. Irminger Water is the warm and saline water mass transported by the NIIC from the Irminger Sea. Polar Surface Water is the cold and fresh water mass transported by the EGC from the Arctic Ocean. The eastern part of the Nordic Seas contains the warmest water masses, while the coldest ones are found in the western part.

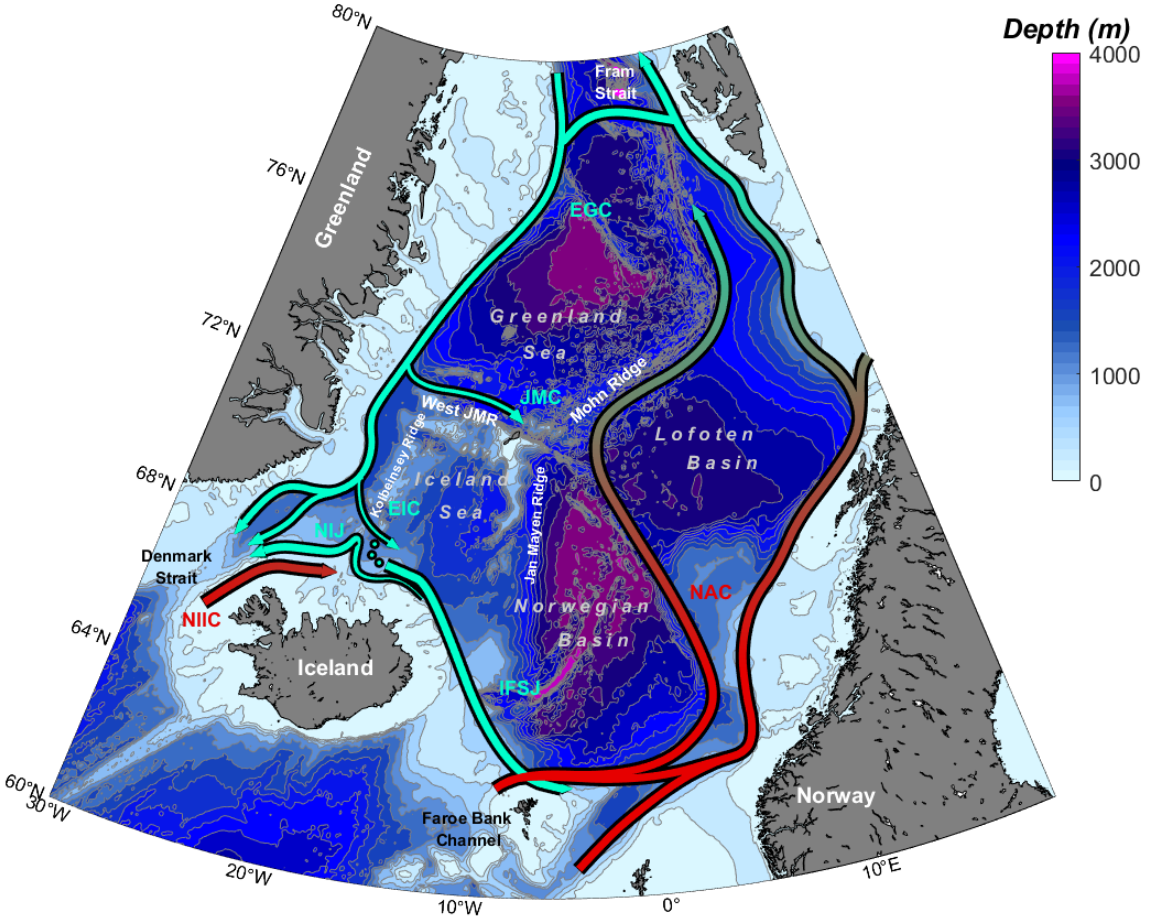

Figure 1.1: Schematic circulation in the Nordic Seas. Cold currents are shown as green arrows, while warm currents are shown as red arrows. The background colors indicate depth levels. The abbreviations are: EGC = East Greenland Current; NAC = Norwegian Atlantic Current; NIIC = North Icelandic Irminger Current; NIJ = North Icelandic Jet; IFSJ = Iceland-Faroe Slope Jet; JMC = Jan Mayen Current; EIC = East Icelandic Current; West JMR = West Jan Mayen Ridge.

1.2 Water mass transformation

1.2.1 Changes in hydrographic properties and structure

The intermediate and deep waters in the Nordic Seas have changed in hydrographic properties and structure since 1950. The deep waters in the Nordic Seas started to warm in the beginning of the 1980s (Østerhus and Gammelsrød, 1999). They concluded that the abyssal warming in the Nordic Seas was not directly connected to global warming. The reasoning for this was that the multidecadal changes in convective intensity in the Greenland Sea appeared to reflect a long-period shift in the North Atlantic Oscillation. The North Atlantic Oscillation is a weather phenomenon with fluctuations in atmospheric pressure at sea level between the Iceland Low and Azores High.

The Greenland Sea has become warmer, more saline and richer in oxygen (Lauvset et al., 2018). The intermediate waters have warmed by 0.63°C and became more saline by 0.036 g/kg since 1986 (Lauvset et al., 2018). The water masses below 2000 m, referred to as deep waters, have warmed by roughly 0.3°C since 1972 (Wang et al., 2015). While the temperature and salinity increased at 2000 m depth, the density decreased (Østerhus and Gammelsrød, 1999).

The Norwegian Sea started to warm later than the Greenland Sea. Lauvset et al. (2018) hypothesized that the Norwegian Sea became warmer and more saline in the beginning of the 2000s, because the inflowing Atlantic Water had increased in temperature and salinity. Both Østerhus and Gammelsrød (1999) and Wang et al. (2015) investigated the temperature changes in the intermediate and deep waters in the Norwegian Basin. The intermediate waters have become warmer by $0.10° - 0.15°$C since 1984 until 2012, while the deep water temperature increased with $0.02° - 0.05°$C.

The Lofoten Basin started to warm in the beginning of the 2000s. The water masses in the 1000 m warmed by 0.39°C from 2011 to 2018 (Mork et al., 2019). Wang et al. (2015) showed that the deep waters (1900–2200 m and 2200–2500 m) increased in temperature by 0.09° and 0.08°C, respectively.

Dense water transported from the Greenland Sea into the Norwegian Sea will sink to a deeper level in the Norwegian Sea. This is because the Greenland Sea contains water masses with higher density than the water masses at the same depth in the Norwegian Sea. The 28.05 kg/m^3 isopycnal was in 2014 located at 660 meters in the Greenland Sea, while it was found at 910 meters in the Norwegian Sea (Shao et al., 2019).

1.2.2 Water mass transformation in the Greenland and Iceland Seas

Convection occurs during winter because of intense heat loss from the surface to the atmosphere. Plumes of dense water sink until they reach a level where their density is the same as the surroundings (Shao et al., 2019). Good conditions for open ocean convection are a cyclonic gyre circulation, weak stratification, and high heat fluxes (Marshall and Schott, 1999). Gyres create doming isopycnals where denser water masses are brought to the surface (Somavilla, 2019). This weakens the stratification in the water column with sloping isopycnals on the sides.

The highest heat loss occurs near the ice edge. The strongest heat loss follows the ice edge as the sea ice retreats away from the gyres in the Nordic Seas (Moore et al., 2015). As the distance from the gyres to the ice edge increase, the heat loss decreases over the gyres which leads to the less favourable conditions for convection. Moore et al. (2015) showed that the ice concentration in the western Iceland Sea has decreased since the 1980s. A further decrease can affect water mass transformation both in the Iceland and Greenland Seas, which in turn may impact the properties and volume transport of the overflows. A change in the overflow might, in turn, affect the supply of dense water to the Atlantic Meridional Overturning Circulation (AMOC).

Dense waters are formed throughout the Iceland Sea, but the densest portions are formed in the northwestern part (Våge et al., 2015). This is because of a stronger atmospheric forcing in this area near the ice edge, compared to the centre of the gyre. Våge et al. (2015) showed that convection in the Iceland Sea has decreased in strength over the last decades and is therefore less likely to supply the densest component of the overflow. Local convection in the Iceland Sea does not reach into the deeper parts because of the high density there, so the origin of the densest water masses supplying the overflows are hypothesized to be the Greenland Sea (Moore et al., 2015).

Convection in the Greenland Sea may be important for the production of denser water masses ($\sigma > 28.03$ kg/m^3), which overflow on both sides of Iceland (Brakstad et al., 2019). Earlier studies proposed that very cold and dense Greenland Sea Deep Water (GSDW) was formed because wintertime deep convection extended almost to the bottom (Aagaard and Carmack, 1989; Carmack and Aagaard, 1973). Since the beginning of the 1980s convection has been limited to intermediate waters (Meincke et al., 1997; Østerhus and Gammelsrød, 1999). GSDW used to prevent other less dense water masses from entering the Greenland Sea at depth because GSDW was denser than the surrounding water masses. When the renewal of GSDW stopped,

lighter water masses were free to enter the Greenland Sea. This is the main reason for the abyssal warming in the Greenland Sea. Meincke et al. (1992) suggested that a decrease of cyclonic wind stress curl and reduction in sea ice formation were factors that diminished convection, while Somavilla (2019) hypothesized that the presence of very fresh water at the surface was a reason for the reduced convection. Meincke et al. (1997) showed that convection in the Greenland Sea was limited to 1000 m depth, and that the GSDW had not been ventilated by local convection in the period 1982-1993.

Moore et al. (2015) found that the Greenland Sea Gyre is experiencing a negative trend in atmospheric forcing which may further reduce the convection from intermediate depth to only shallow depth. In the mid 1990s, a new class of intermediate water started to develop in the Greenland Sea. This water mass is less dense than the GSDW and was first discovered by Malmberg (1983). This new water mass has been called Greenland Sea Arctic Intermediate Water (GSAIW), and the new class of GSAIW has since 1994 been the main product of convection in the Greenland Sea. Since then, an increase in near-surface salinity has weakened the stratification in the Greenland Sea, and, together with strong atmospheric forcing, resulted in convection exceeding 500 m and thus formation of GSAIW (Brakstad et al., 2019).

1.3 Overflows

Plumes of dense water formed in the Nordic Seas spill over the GSR and contribute to the densest portion of the AMOC (Eldevik et al., 2009; Hansen et al., 2016). Approximately one-third of the total overflow water flows through the FBC (Hansen et al., 2016), while most of the remainder flows through Denmark Strait (Jochumsen et al., 2017). Between Iceland and the Faroe Islands water spills over the Iceland-Faroe Ridge (IFR) into the Atlantic Ocean (Hansen et al., 2016). However, the contribution from the IFR to the total overflow is small. A small portion of the total overflow is also crossing the Wyville Thompson Ridge south of the Faroe Islands.

1.3.1 Faroe Bank Channel Overflow

Est of Iceland passes most of the densest water masses through the FBC. The average volume transport through the FBC is around 2 Sv (Hansen et al., 2016). At the ridge, the FBC overflow plume is the deepest and densest, but entrainment of ambient waters downstream of the sill ultimately makes the FBC overflow less dense than the Denmark Strait overflow water (Hansen et al., 2016).

1.3.2 Denmark Strait Overflow

The largest transport of dense overflow water from the Nordic Seas takes place in Denmark Strait (Jochumsen et al., 2017). The average overflow transport through Denmark Strait is roughly 3.2 Sv (Jochumsen et al., 2017). Through both Denmark Strait and the FBC water flows in near the surface and out at depth. A density contrast between these two layers and sloping isopycnals creates a baroclinic pressure gradient that accelerates the currents toward the overflows (Hansen et al., 2008). This means that the Nordic Seas act as a reservoir of dense water for the Atlantic Ocean and the overturning circulation there is driven by the pressure gradient.

1.4 Pathways of overflow water

The main contributors to the Denmark Strait Overflow Water are the EGC and the North Icelandic Jet (NIJ). The EGC separates into two branches north of Denmark Strait called the separated EGC and the shelfbreak EGC (Figure 1.1; Våge et al., 2013). Roughly 30% of the Denmark Strait Overflow Water is transported by the NIJ, while the two branches of the EGC transport the remaining 70% (Harden et al., 2016). Later on, Semper et al. (2019) showed that the NIJ can account up to 50% of the Denmark Strait Overflow Water. The NIJ transports the densest water toward Denmark Strait and is found in the deepest part of the sill (Mastropole et al., 2017). While the EGC transports warm and salty Atlantic-Origin water, the NIJ transports colder, fresher and denser water of Arctic origin (Section 1.1.3; Våge et al., 2011). The NIJ merges with the separated EGC north of Denmark Strait (Semper et al., 2019).

One of the main contributors of overflow water to the FBC is the Iceland-Faroe Slope Jet (IFSJ; Figure 1.1). Semper et al. (in review) hypothesized that roughly half of the overflow transport through the FBC is supplied by the IFSJ.

1.4.1 The North Icelandic Jet

The NIJ was first observed along the Iceland slope by Jónsson (1999) and Jónsson and Valdimarsson (2004). The narrow current is mid-depth intensified and only 15–20 km wide with a typical velocity around 40 cm/s (Jónsson and Valdimarsson, 2004). The jet is usually situated above the 650 m isobath, which is also the depth of the Denmark Strait sill (Våge et al., 2011). Semper et al. (2019) showed that the NIJ has a double-core structure, with the inner core located at roughly 600 m depth and the outer core at roughly 800 m depth. Temperature and salinity measurements of the NIJ at sections across the Icelandic slope can be put into a $\theta - S_A$ diagram. All the profiles have one density value, and by doing a transport-weighted average of all the values the transport mode is obtained (Semper et al., 2019). The transport-weighed average contain all the density values that belongs to the bulk of the dense water masses transported by the NIJ. The NIJ transport mode is $-0.29° \pm 0.16°$C in temperature and 35.075 ± 0.006 g/kg in salinity (Semper et al., 2019). These properties correspond to a potential density of 28.05 kg/m^3. There is no sign of long term variability in the current, but it has high variability on short time scales of a couple of days (Jónsson, 1999; Semper et al., 2019). The deepest part of the NIJ has warmed by more than 0.15°C over a nine-year period from 2004 to 2013 (Pickart et al., 2017).

1.4.2 The Iceland-Faroe Slope Jet

The IFSJ is a narrow, bottom-intensified current flowing along the Iceland-Faroe slope, with two cores located at the 750 and 1100 m isobaths (Semper et al., in review). This current carries mainly cold, dense water, which is banked up against the slope. The dense water which banks up along the Icelandic slope and IFR is consistent with the mid-depth intensification of the NIJ and the bottom intensification of the IFSJ. The transport mode of the IFSJ is $-0.52° \pm 0.11°$C in temperature and 35.075 ± 0.003 g/kg in salinity, which corresponds to a density of 28.06 kg/m^3 (Semper et al., in review). It has been hypothesized that the NIJ and IFSJ have the same source because of the similarities in their properties (Semper et al., in review).

1.5 Origin of the densest overflow water

The NIJ was originally thought to originate in the Iceland Sea (Jónsson, 1999; Jónsson and Valdimarsson, 2004). Våge et al. (2011) hypothesized that the NIJ is part of a local overturning cell that involves the boundary current system north of Iceland and water mass transformation in the central

Iceland Sea. The NIIC transports warm Irminger Water northward through Denmark Strait, before the current disintegrates northeast of Iceland. The warm water is transformed into denser water by open-ocean convection in the Iceland Sea (Section 1.2.2), which was thought to feed the NIJ (Våge et al., 2011; Pickart et al., 2017).

However, Våge et al. (2015) later found that the central Iceland Sea is not the origin of the densest water advected by the NIJ. The lack of dense mixed layers in the Iceland Sea indicates that local convection is not an important source of the densest overflow water. Våge et al. (2015) also showed that dense water was formed outside the gyre, in the northwestern Iceland Sea (Section 1.2.2). Dense water originating outside the gyre has a more direct pathway to the NIJ compared to water from the centre of the gyre. But dense water formed in the northwest Iceland Sea is also not dense enough to be considered a main source of the NIJ (Pickart et al., 2017; Våge et al., 2015).

Brakstad et al. (2019) suggested that the Greenland Sea is an important source of dense water to the NIJ. They suggest that in recent winters around 0.6 ± 0.5 Sv of water denser than 28.05 kg/m^3 formed within the Greenland Sea gyre. This is roughly half of the amount that the NIJ is transporting (Semper et al., 2019). A recent study indicates that both the NIJ and IFSJ are fed by dense water originating from the Greenland Sea, flowing through the Iceland Sea along the Kolbeinsey Ridge and the Jan Mayen Ridge (Huang et al., in review). The authors concluded that the Greenland Sea is the main region where ventilation of the densest overflow water occurs.

1.6 Motivation for this study

Dense water formation in the Greenland Sea has been important for the general circulation in the Nordic Seas and as a source of dense water to the lower limb of the AMOC (Eldevik et al., 2009; Hansen et al., 2016). After the bottom convection ceased in the 1980s, the Greenland Sea started to change in structure and properties. The Greenland Sea has become warmer and saltier over the last decades (Section 1.2.1; Lauvset et al., 2018; Brakstad et al., 2019). In the first part this study focuses on how the hydrographic properties of the intermediate and deep waters in the Nordic Seas have changed from 1950 to 2018 using an extensive collection of historical hydrographic data (Section 2.1). By comparing different areas in the Nordic Seas, the objectives are to identify the origins of the deep and intermediate warming in the Nordic Seas and clarify the importance of the Greenland Sea.

Previous studies have suggested that the dense water formed in the

Greenland Sea is the source of both the NIJ and IFSJ (Semper et al., in review; Huang et al., in review). Both the NIJ and IFSJ transport substantial amounts of dense water ($\sigma > 28.03$ kg/m^3) towards the GSR and are important for the overflows. Changes in the Nordic Seas, especially in the Greenland Sea, could impact the hydrographic properties of the overflows and the AMOC. In the second part of the thesis I will focus on how the properties of the NIJ and IFSJ have changed from 1950 to 2018. The aim is to determine whether these changes can be traced back to the Greenland Sea.

Chapter 2

Data and Methods

2.1 Hydrographic data

The hydrographic data set is based on the Unified Database for Arctic and Subarctic Hydrography (UDASH), which covers the Nordic Seas north of 65°N from 1980 to 2015 (Behrendt et al., 2017). Data from other sources such as the World Ocean Database (WOD) and the International Council for the Exploration of the Seas (ICES) are added to cover areas outside the UDASH domain, before 1980 and after 2015 (Brakstad et al., in prep). The collective data set, covering the domain 60–80°N and 30°W–18°E, has further been augmented by data listed below:

- Marine and Freshwater Research Institute in Iceland (MFRI) data set from 1950–1990 (Palsson et al., 2012)
- Norwegian Iceland Seas Experiment database (NISE) data set (Nilsen et al., 2008)
- Faroe Marine Research Institute (FAMRI) data set from 1987–2018

The observational data along the Iceland slope collected before 1988 were taken by water bottles. From 1988 onwards, the Icelandic data were obtained by a Conductivity-Temperature-Depth (CTD) instrument. The remaining data were obtained by CTD from 1990, with water bottle sampling before 1980. Between 1980 and 1990 both methods were used, with gradually increasing use of CTD. Duplicate profiles have been removed, all profiles have been quality controlled and required to contain both temperature and salinity measurements. The quality check involves removing erroneous profiles, density inversions, and outliers, according to Skagseth and Mork (2012),

Våge et al. (2013, 2015) and Brakstad et al. (2019). The spatial and temporal distribution of the data are shown in Fig. 2.1.

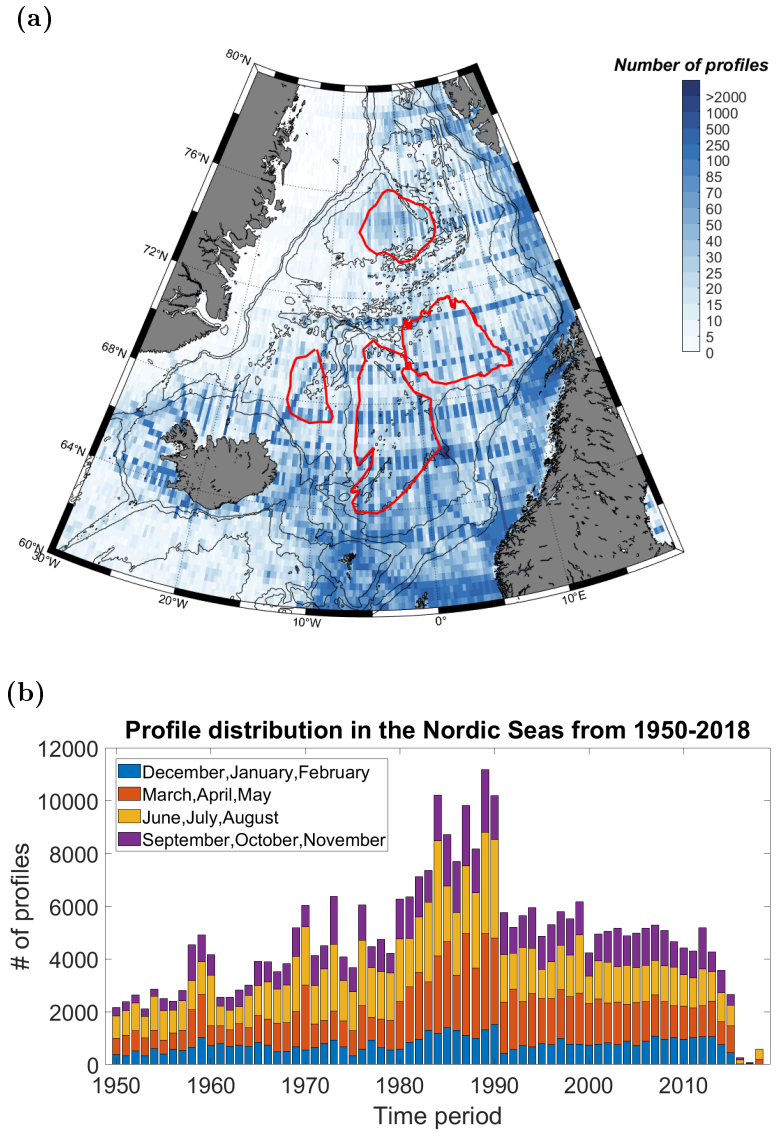

Figure 2.1: (a) Spatial and (b) temporal overview of profiles in the Nordic Seas. (a) The colors indicate the number of profiles within a grid cell of 0.25° latitude by 0.25° longitude. The gyres and basins are outlined by red contours, and the black contours are the 500, 1000, 2000, 3000, and 4000 m isobaths. (b) The bars show the annual number of profiles from 1950 to 2018. The seasons are indicated by different colors, blue is winter, red is spring, yellow is summer, and purple is autumn.

2.2 Methods

2.2.1 Thermodynamic Equation Of Seawater - 2010

The Thermodynamic Equation Of Seawater–2010 (TEOS–10) standards were first defined in 2010, superseding the older 1980 International Equation of State of Seawater (EOS–80). The most significant change between EOS–80 and TEOS–10 is the use of Absolute Salinity instead of practical salinity. This change means going from practical salinity unit (psu) to g/kg. TEOS–10 is based on mass fractions of salt in sea water, while EOS-80 uses the measured conductivity in the sea water. TEOS–10 also provides a more complete representation of the thermodynamic properties of sea water. Some other advantages using TEOS–10 compared to EOS–80 are that TEOS–10 uses the latest temperature standards, which gives a more consistent description of sea water, and TEOS–10 has more accurate values for sea water properties. The Gibbs Sea Water Functions (GSW) data package for MATLAB (McDougall and Barker, 2011) provides functions to convert the data to TEOS–10 standards. Depth was calculated from pressure, and surface pressure was used as a reference in calculations of potential spicity and potential density.

2.2.2 Potential spicity and Sigma-Pi distance

Previous publications have sought to define a thermodynamic variable that is orthogonal to potential density. Such a variable would provide different information about temperature and salinity compared to potential density (Huang et al., 2018). Spiciness or spicity was first proposed by Munk (1981). Potential spicity describes spatial changes in temperature and salinity along a constant isopycnal, and it is a result of air-sea fluxes, turbulent mixing, and advection (Todd et al., 2012). At the same reference pressure, potential density (σ) and potential spicity (π) are orthogonal (Huang et al., 2018). The calculation of potential spicity depends on temperature, salinity, and a reference pressure. Huang et al. (2018) defined a variable called Sigma-Pi ($\sigma - \pi$) distance, which is the shortest distance in potential density–potential spicity space between two water parcels. Since the potential density and potential spicity gradients are of the same magnitude, the $\sigma - \pi$ space is meaningful to use for calculations of distance. The $\sigma - \pi$ distance can be used to investigate how water masses have changed or to track water masses back to the source. From the potential spicity and the potential density of two different water masses, the $\sigma - \pi$ distance is calculated using the following equation:

$$\mathrm{D}_{1,2} = \sqrt{(\sigma_1 - \sigma_2)^2 + (\pi_1 - \pi_2)^2}, \tag{2.1}$$

where (σ_1,π_1) and (σ_2,π_2) are the properties of the two water parcels referenced to the sea surface pressure (Huang et al., 2018). All three variables have the same unit (kg/m^3).

2.2.3 Stations and areas

Changes in hydrographic properties can be examined by defining the four basins in the Nordic Seas. The Norwegian and Lofoten Basins are defined by the 3000 m isobath (Dugstad et al., 2019). The Greenland Sea and Iceland Sea gyres are defined following Moore et al. (2015), who used dynamic topography of the surface relative to 500 m to outline the gyres. There are several repeated stations that are part of hydrographic survey programs from the MFRI and the FAMRI, where the locations shown in Table 2.1.

Table 2.1: Coordinates for the repeated stations

Station	Latitude [°N]	Longitude [°W]
Kögur 5	67.30	23.62
Sletta 5	67.73	16.15
Siglunes 8	68.00	18.83
Station 5	63.00	06.08
Jan Mayen Channel	71.15	07.30

A band along the Icelandic slope and the IFR is defined by the 500 and 900 m isobaths along the Icelandic slope, and by the 600 and 1300 m isobaths along the IFR. Along the IFR the isobaths are chosen to cover the IFSJ, which follows the 750 and 1100 m isobaths. The isobaths along the Icelandic slope are chosen to cover the two cores of the NIJ, which are located at around 600 and 800 m. The stations and areas are highlighted in Figure 2.2.

2.2.4 Time series

In most years, the repeated stations have been sampled several times per year. By averaging over each year a mean annual profile is obtained. The annual profiles are further reduced to a scalar value by averaging over a depth or density interval. Only profiles that contain more than five data points within the interval were included in the calculations. The density interval of 28.04 – 28.06 kg/m^3 was selected because this is the range of the transport mode of the NIJ. Depth intervals have been chosen to cover the depths where the transport mode of the NIJ is roughly located at each of the

stations (KG5 = 380–480 m, SI8 = 650–750 m and SL5 = 570–670 m). Depth intervals for intermediate waters in the Greenland Sea Gyre were defined by typical mixed-layer depths (500–1500 m) in this basin as identified by (Brakstad et al., 2019). This corresponds to approximately a density interval of 28.04 – 28.07 kg/m^3. Water masses below 2000 m in the Greenland Sea were considered deep waters. The density range from the depth interval in the Greenland Sea was used to define depth intervals including the same density range in the Iceland Sea, Lofoten, and Norwegian Basins.

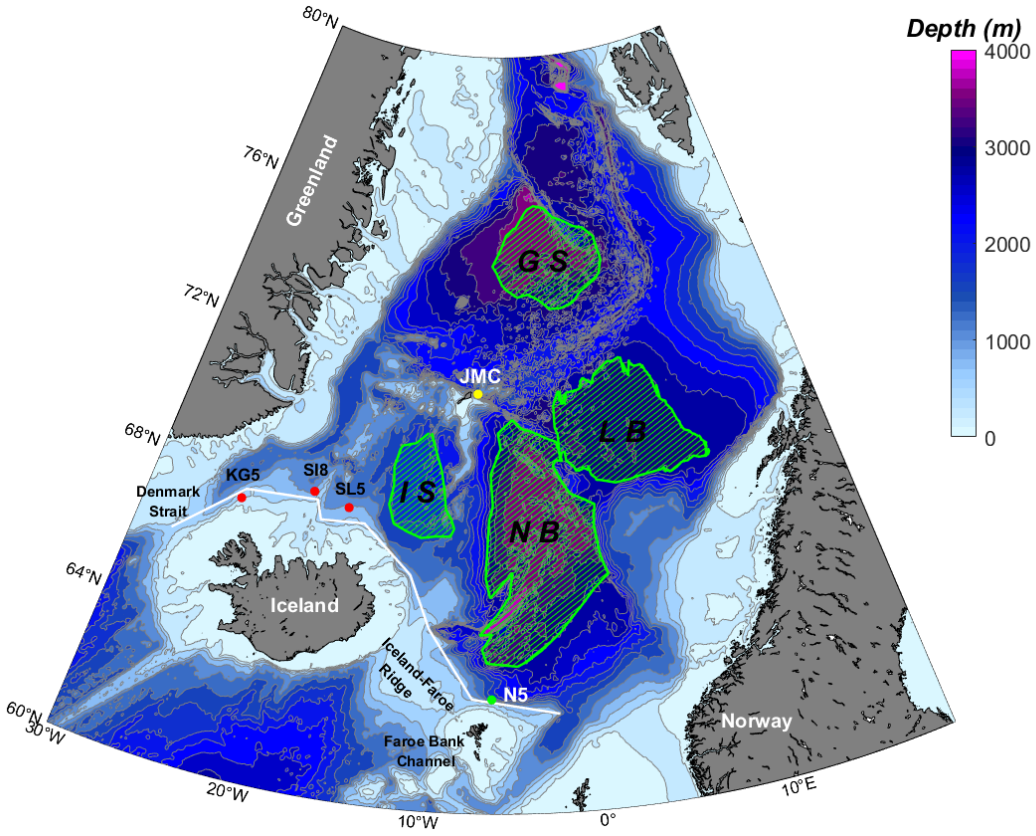

Figure 2.2: Map of the areas and repeated stations in the Nordic Seas that are used in the analysis. The background color shows depth levels. The white line along the slope represents the band along the Icelandic slope and the IFR. The colored dots show the repeated stations. The abbreviations are: GS = Greenland Sea, IS = Iceland Sea, NB = Norwegian Basin, LB = Lofoten Basin, JMC = Jan Mayen Channel station, KG5 = Kögur station 5, SI8 = Siglunes station 8, SL5 = Sletta station 5 and N5 = Section N station 5.

The data have been linearly interpolated onto a regular vertical coordinate to obtain a data set with equal vertical resolution. A trend for each variable is calculated from a piecewise linear least squares fit method (Albertin, 2020). This method calculates a linear trend for continuous time series and defines breakpoints along the x-axis where the deviation between the trend and the data are smallest. All time series include the following variables: Conservative Temperature, Absolute Salinity (hereafter temperature and salinity), potential spicity, $\sigma - \pi$ distance (between a chosen water mass and the transport mode of the NIJ), and either depth (for density intervals) or potential density (for depth intervals).

2.2.5 Vertical grids

The hydrographic data were interpolated onto regular 5 km by 10 m or 10 day by 10 m grids using a Laplacian-spline interpolator (Pickart and Smethie, 1998). All data points outside of the $\pm$ 3 standard deviation envelope were identified as outliers and removed before creating the grid. This is a standard procedure for identifying outliers (Thomson and Emery, 2014).

For the band along the Icelandic slope and the IFR, vertical grids were created as follows: First, the distance along the band was calculated. Second, the distance from Denmark Strait to each station was calculated. Third, for every 150 km along the band a box was created. All profiles located inside each box were used to create an average station for each box. Lastly, after obtaining one average station per 150 km along the band, these were used for further analysis. The intervals of 150 km give a smooth horizontal resolution in distance along the Icelandic Slope and IFR.

2.2.6 Horizontal grids

Currents tend to follow bathymetry, or f/H contours. f/H is potential vorticity, where f is the Coriolis parameter ($f = 2\Omega\sin\varphi$, φ is latitude) and H is the height of the water column. The hydrographic properties are most similar along depth levels and the likelihood of changes in the hydrographic properties is larger when crossing isobaths. This is the main reason for the use of an anisotropic gridding routine. By creating an anisotropic grid, the routine elongates the search radius along bathymetry to maximize the information collected from the same depth as the grid point (Våge et al., 2013). The routine is capable of taking anisotropy in the form of bathymetry or f/H contours into account. When the planetary vorticity is weak the f/H field is dominated by topography, which is the case in the Nordic Seas where circulation and bottom contours also are in close alignment (Nøst and Isach-

sen, 2003). Hence, in regions with large topographic gradients, the effective radius r is increased along isobaths to consider the greater correlation length scales along the bottom topography. The distance r between the grid and the observational points can be calculated by differences in bottom depths:

$$r^2 = {r_x}^2 + {r_y}^2 + \left(\lambda * \frac{H_a - H_o}{H_a + H_o}\right)^2 \tag{2.2}$$

The variables r_x and r_y are the geographic distances between the observation and analysis points in the zonal and meridional directions, while H_a and H_o are the bottom depths of the analysis and observation points (Skagseth and Mork, 2012). The topography parameter (λ) minimizes the across-bathymetry correlation in regions where currents are impacted by topographic gradients (Lavender et al., 2005). Increments of 0.25 degrees in the zonal and meridional directions are used. This grid routine has been used in previous studies (e.g Skagseth and Mork, 2012; Voet et al., 2010; Våge et al., 2013; Lavender et al., 2005).

2.2.7 Volume and density classes

The Nordic Seas have been divided into cells in zonal and meridional directions with increments of 0.25 degrees (Figure 2.1a). All the profiles were binned depending on the location of the profile. A vertical coordinate with 42 elements was created, ranging from 0 to 4000 m. For the shallower areas such as the Iceland Sea, was the vertical coordinate reduced to only extend to the maximum depth of the area. The vertical coordinate was combined with the horizontal cells so that each horizontal cell included several vertical layers. Density classes were created, ranging from 20 to 28.4 kg/m^3 with increments of 0.01 kg/m^3. The volume and average density of each three dimensional cell was then estimated. Thereafter the volume per density class was calculated from all cells in both horizontal and vertical directions. The total volume of the entire area was obtained by summing together all the density classes, before the volume of each density class was divided by the total volume of the area to facilitate comparison between areas.

2.3 Uncertanties

There are some uncertainties concerning the data collection and methods that need to be addressed. The extensive data collection (Section 2.1) was collected by both CTD and water bottle samples. The older data collected by water bottles, include a bigger uncertainty compared to the data from the

CTD. The CTD data have uncertainty less dense 0.005°C for temperature and 0.01 g/kg for the salinity. The different methods used throughout this thesis also include some uncertainties, such as calculating the trends or calculating the volume of the density classes. For some of the time series are the trends calculated over periods containing both CTD and water bottle data. This will then increase the uncertainties of those estimates. The annual average could also imply some uncertainty in the results, because it adds all the profiles from one year. The convection happens only during winter, and by adding all months, the resulting signal can be different compared to only winter or summer. But overall, the biggest uncertainties are related to the difference in data collecting over the entire period.

Chapter 3

Results

This chapter is divided into two parts. The first part demonstrates how the Nordic Seas have changed in hydrography and structure from 1950 to 2018. The second part of the chapter focuses on how the hydrographic properties of the NIJ and IFSJ have changed from 1950 to 2018.

3.1 Hydrographic changes in the Nordic Seas

3.1.1 Temperature and salinity

Lateral maps of temperature and salinity at 1200 m depth are shown in Figure 3.1). The depth of 1200 m was chosen because this depth level was located within all the depth intervals for the four basins (Greenland Sea = 500–1500 m; Iceland Sea = 600–1700 m; Lofoten Basin = 1000–2000 m; Norwegian Basin = 750–1750 m). The depth level was also acting as an upper limit for the warming around 2000 for the entire water column in the basins, except the Greenland Sea (Section 3.1.2). In the first period (1980–1999; Figure 3.1a), the Greenland Sea Gyre had the lowest temperatures. The water masses in the Lofoten Basin were warmest with temperatures close to 0°C. In the period from 2000 to 2018 the Greenland and Iceland Seas contained the coldest water masses at 1200 m (Figure 3.1c). The Lofoten Basin was still the warmest area, while the Norwegian Basin did not change significantly from the first period. The entire Nordic Seas became warmer from the first (1980–1999) to the last (2000–2018) period (Figure 3.1e). The Greenland Sea had the highest temperature increase at 1200 m depth.

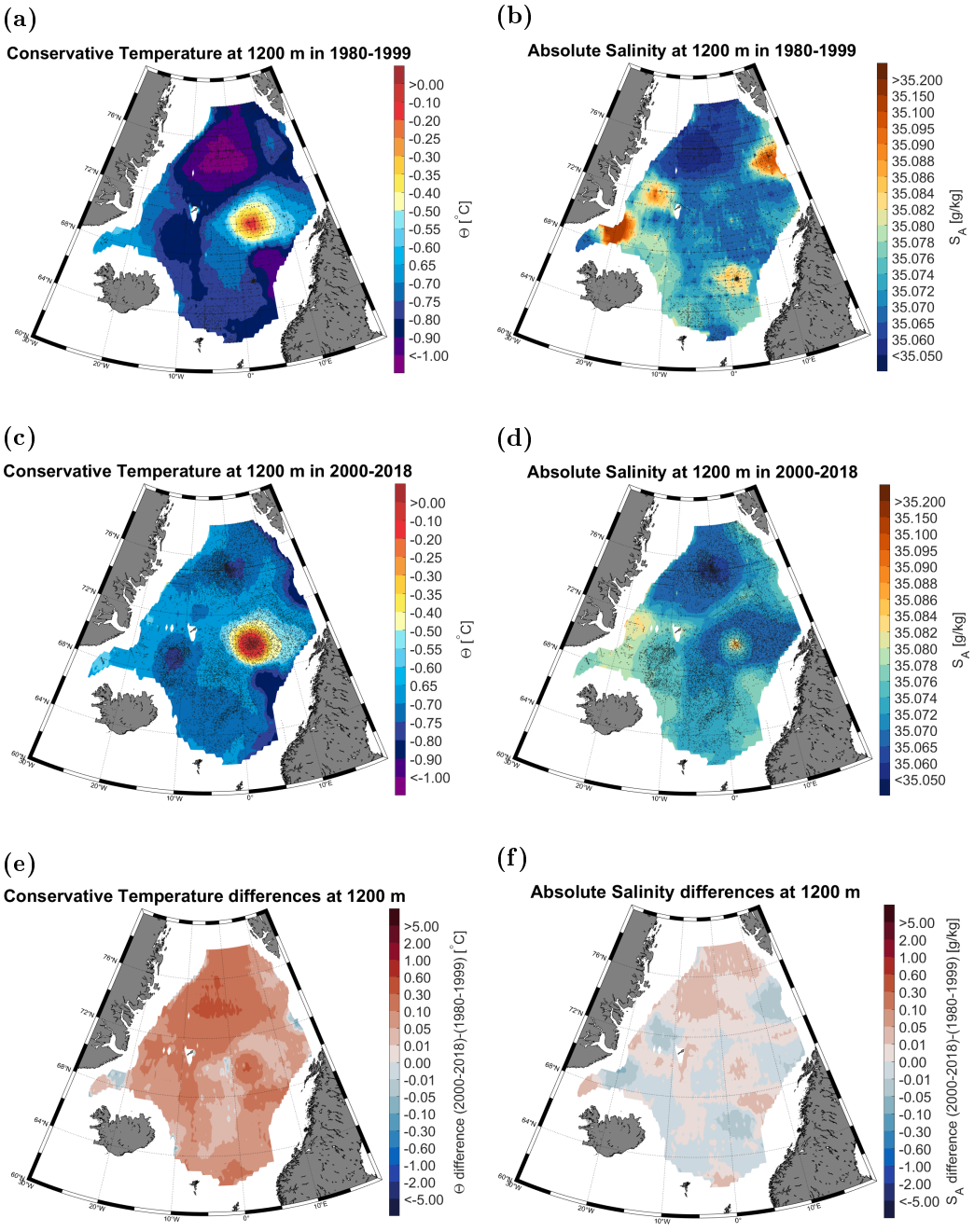

Figure 3.1: Temperature (left panels) and salinity (right panels) in the Nordic Seas at 1200 m depth. The different panels show mean values during the period 1980–1999 (a-b), mean in 2000–2018 (c-d), and the difference between these two periods (e-f). The blue color indicates a decrease, while the red color indicates an increase from the first to the last period [(2000–2018) - (1980–1999)]. The black dots (a-d) show the locations of the profiles.

The salinity field in 1980-1999 (Figure 3.1b) shows that the Greenland Sea Gyre contained the freshest water masses at 1200 m depth. The Norwegian Basin was the basin with the highest salinity. The water masses in both the Greenland Sea Gyre and the Lofoten Basin increased substantially in salinity in the last period (2000–2018) compared to the first period (1980–1999), although the freshest water masses were still found in the Greenland Sea. The Iceland Sea also became more saline, while the Norwegian Basin showed signs of becoming fresher. A freshening of the upper 1000 m in the Norwegian Basin was also observed by Mork et al. (2019).

I investigated the temporal evolution of temperature and salinity in the four basins more closely, in particular the intermediate and deep water masses (Figure 3.2a). The mixed-layer depth in the Greenland Sea corresponds an approximate density range of 28.04 – 28.07 kg/m^3. This density range was used to determine the different depth intervals in the Iceland and Norwegian Seas (Figure 3.2).

Starting in the 1980s both intermediate (500–1500 meter) and deep waters (below 2000 meter) became warmer in the Greenland Sea (Figure 3.2a). Prior to that the intermediate waters cooled in the 1970s, before the temperature suddenly increased rapidly. The temperature of the intermediate waters in the Greenland Sea increased from around –1.25° to –0.4°C from 1984 to 2016. This corresponds to a warming rate of 0.21 ± 0.07°C/decade. From 1986 the deep waters warmed by 0.14 ± 0.04°C/decade. The water masses between 600 and 1700 m in the Iceland Sea first started to warm in the beginning of the 1990s with a slower rate (0.05 ± 0.14°C/decade) compared to both water masses in the Greenland Sea. Both basins in the eastern part of the Nordic Seas also became warmer. The Norwegian Basin started to warm a couple of years before the Lofoten Basin with a warming rate of 0.05 ± 0.23°C/decade. A warming by 0.046°C/year in the upper 1000 m in the Norwegian Basin was documented by Mork et al. (2019).

A salinity increase in the Greenland Sea was observed corresponding to the increase in temperature (Figure 3.2b). From 1960 to the beginning of the 1980s all of the basins became less saline. The intermediate waters in the Greenland Sea then increased in salinity from 1984 by $(0.84 \pm 1.7) * 10^{-2}$ g/kg per decade, while the deep waters became more saline from 1986 at a rate of $(1.0 \pm 1.2) * 10^{-2}$ g/kg per decade. The other basins remained roughly constant from the 1990s.

From the beginning of the 1970s to the 1990s the density of the intermediate and deep waters decreased. From 1990 all of the water masses, except the deep waters in the Greenland Sea, became lighter. The deep waters in the Greenland Sea remained fairly constant in density for the rest of the period (not shown).

(a)

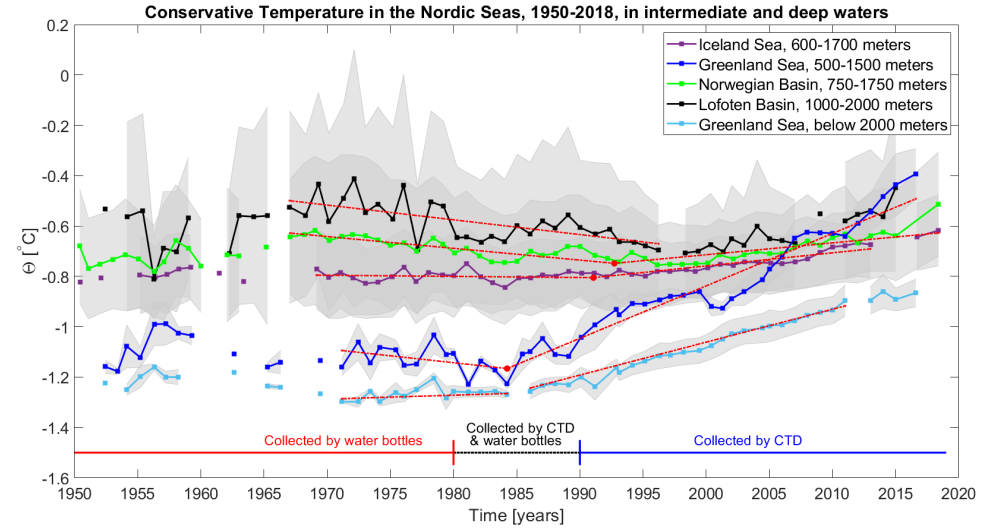

(b)

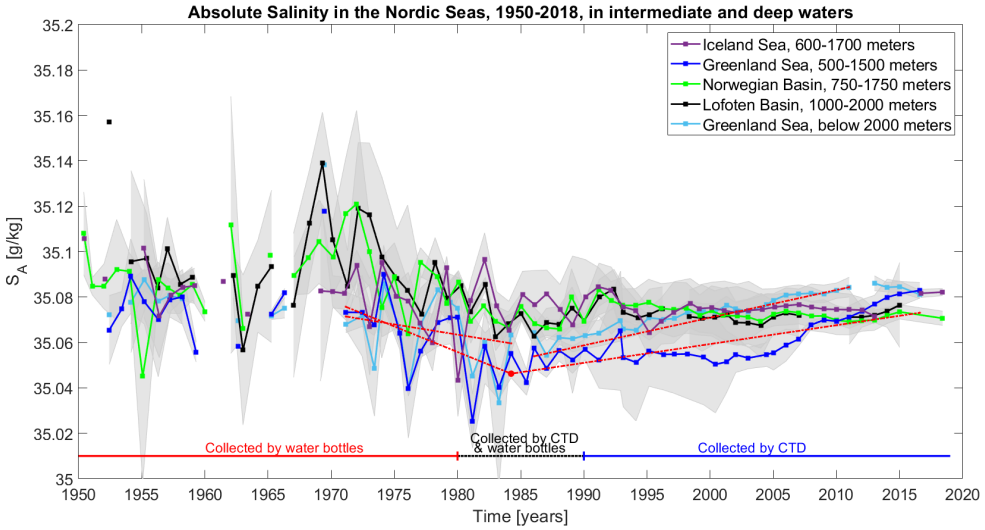

Figure 3.2: Temperature (a) and salinity (b) time series from 1950 to 2018 in the four different basins of the Nordic Seas. The lines represent the intermediate and deep waters in the basins that correspond to the density range of the 500-1500 m layer in in the Greenland Sea. The grey shading shows the standard deviation. The red dashed lines show the trends, while the red points mark the breakpoints (Section 2.2.4).

3.1.2 Temperature changes through the water column

After focusing on the mean properties of different water masses, in this section temperature changes throughout the water column in the different basins will be investigated. Comparing the different basins can help to identify where and when the warming started in the different basins. The anomalies are calculated relative to an average profile for the entire time period.

The warming trend first started in the Greenland Sea (Figure 3.3a). In the period 1950-1980 the upper 1000 m consisted mainly of water masses colder than 0.5°C. From around 1980, the warming signal started to emerge and it progressed deeper into the water column with time. Water colder than –1°C disappeared from the Greenland Sea around 2010. The temperature anomalies indicate that the water masses below 2000 m started to change around 1985 (Figure 3.3b). From around 1995, the whole water column became warmer.

After 1995 warmer water masses slowly started to emerge also in the Iceland Sea (Figure 3.4a), where a warming near the surface and below 1000 m was first observed. 15 years after the warming started, the whole water column was anomalously warm (Figure 3.4b).

The coldest water masses in the Norwegian Basin were located below 2000 m until 1990 (Figure 3.5a). In 1990 the water masses below 2500 m started to warm (Figure 3.5b). The rest of the period showed a warming trend, experienced by more and more of the water column. In the middle of the 2000s the coldest (< -1°C) water masses had disappeared and the entire water column below 1200 m was anomalously warm.

A couple of years after the Norwegian Basin started to warm, the Lofoten Basin experienced the same changes. The warming signal deepened from the beginning of the 1990s and the coldest water masses were located deeper. In the beginning of the 2000s, the coldest water masses disappeared. The deepest part started to warm from around 1992 (Figure 3.6b). By the beginning of the 2000s the entire water column below 1500 m was anomalously warm, and this warming trend continued until the end of the period.

The warming signal started in the Greenland Sea, before the other basins started to warm within ten years afterwards. The deep water in the Greenland Sea started to change in 1985, before the entire water column became warmer around 1995. The other basins started to warm at depth, before the warming signal spread upwards over time.

(a)

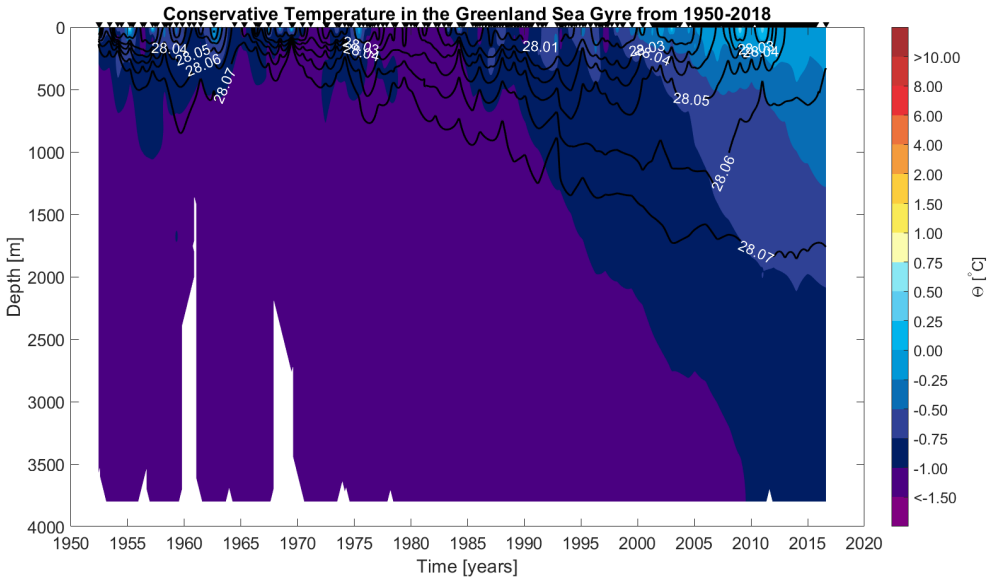

(b)

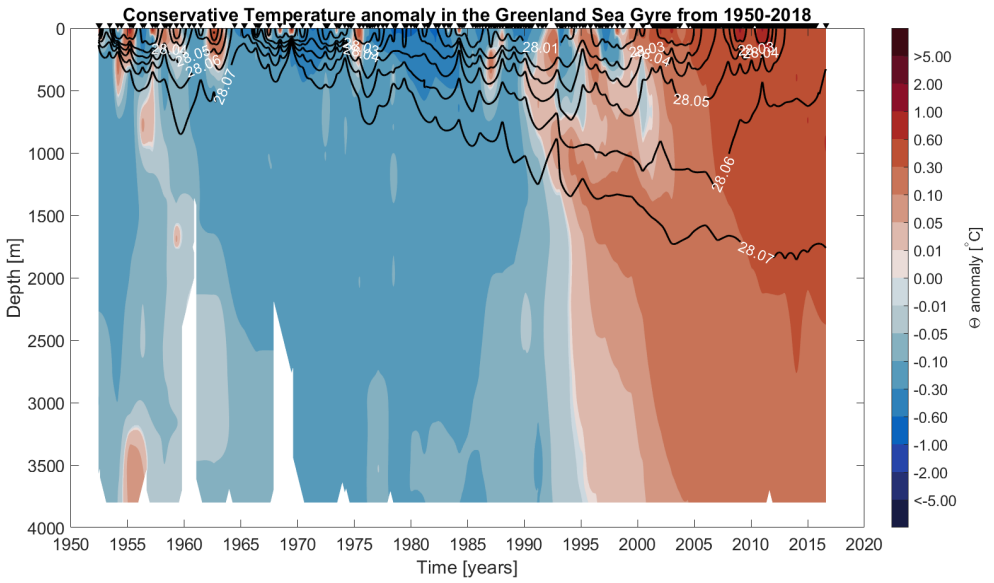

Figure 3.3: Temperature (a) and temperature anomalies (b) relative to the mean profile from the Greenland Sea Gyre from 1950 to 2018. The black lines are the 27.8, 28.01, and 28.03 – 28.07 kg/m^3 isopycnals. The black triangles on the top represent the profiles in the basin. For the anomalies red color indicates temperature increase, while blue color indicates temperature decrease.

(a)

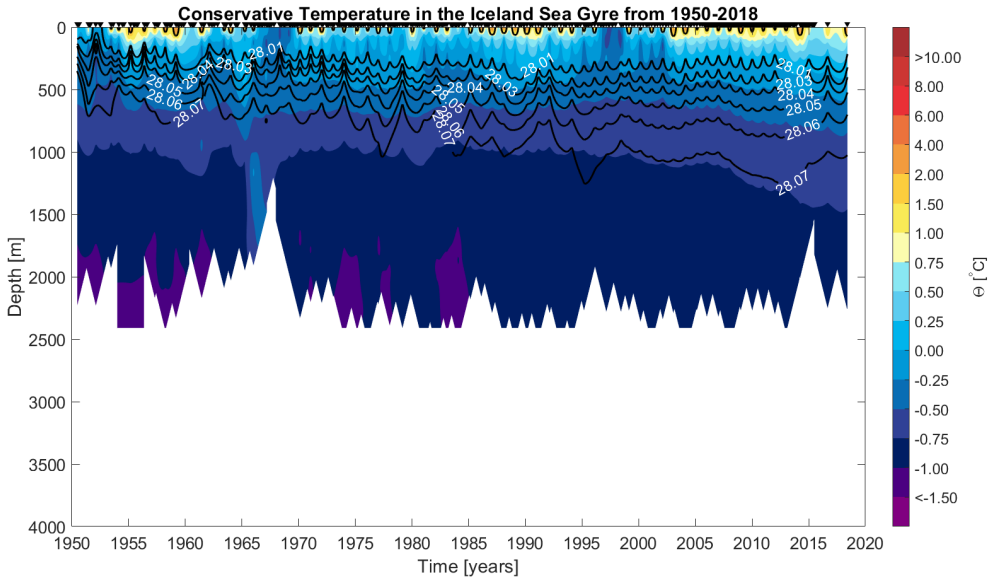

(b)

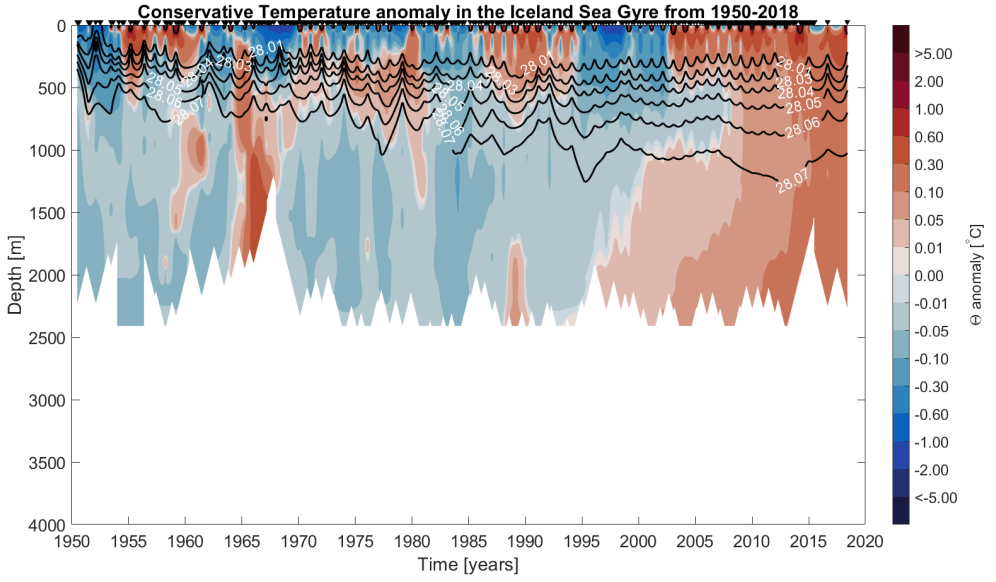

Figure 3.4: As for Figure 3.3, but only for the Iceland Sea Gyre

.

(a)

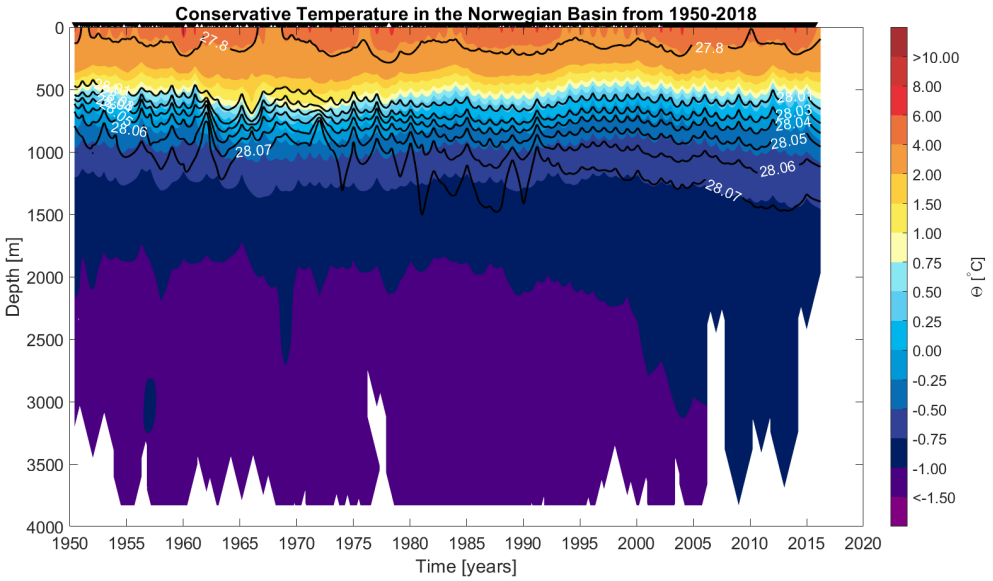

(b)

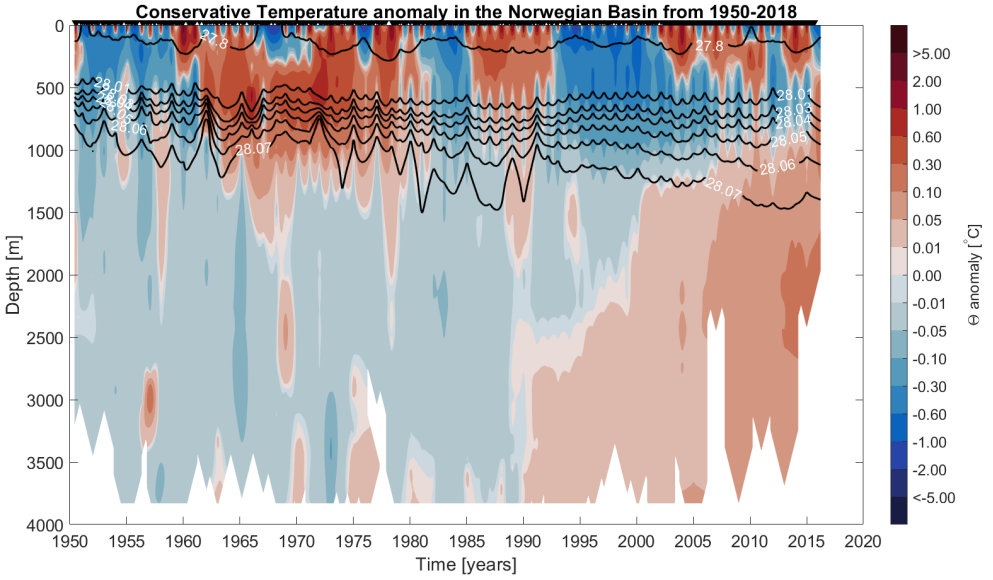

Figure 3.5: As for Figure 3.3, but only for the Norwegian Basin

.

(a)

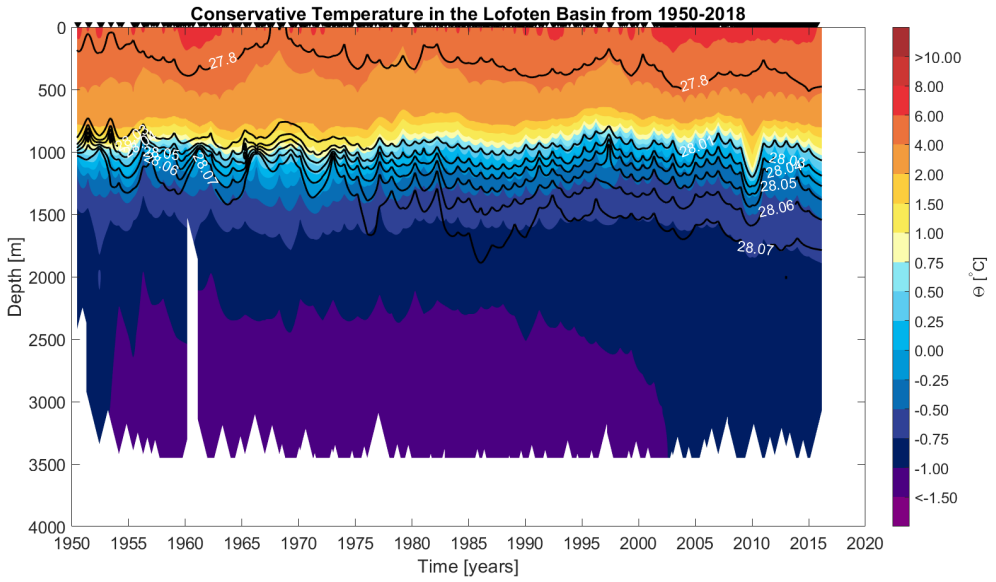

(b)

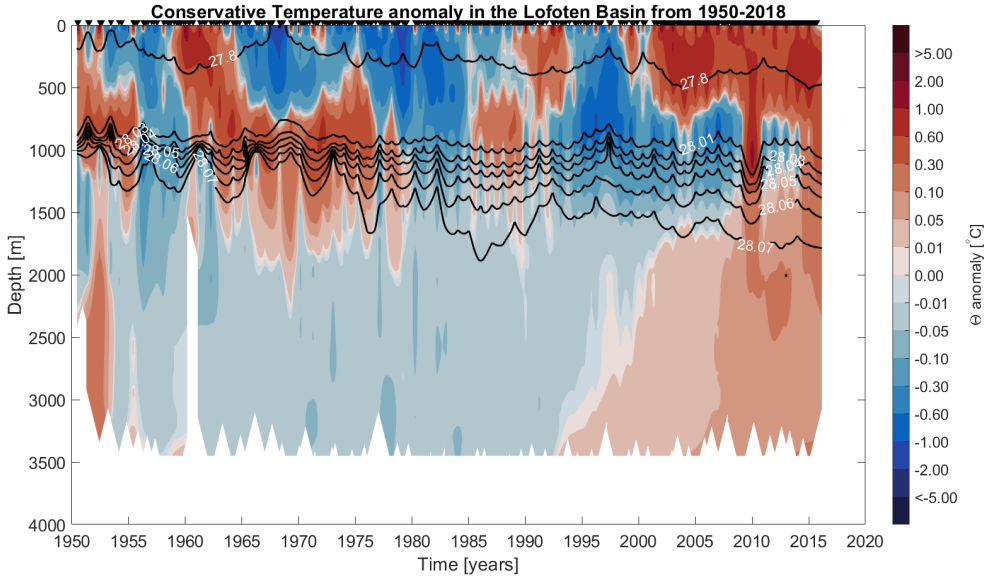

Figure 3.6: As for Figure 3.3, but only for the Lofoten Basin

.

3.1.3 Change in the density structure of the Nordic Seas

Potential density anomalies in the four basins are shown in Figure 3.7 and 3.8. These are relative to average profiles over the entire period. The density in the Greenland Sea (Figure 3.7a) started to decrease in the beginning of the 1980s. The water masses below 1500 meters first became less dense, before the whole water column decreased in density and contained less dense water masses. The water column in the Iceland Sea (Figure 3.7b) became more stable with lighter water masses above denser water masses. The water column decreased in density in 1995 and became anomalously less dense for the rest of the period. The Norwegian Basin (Figure 3.8a) decreased in density roughly at the same time as the Greenland Sea. From the beginning of the 1980s, the deeper water masses became anomalously lighter before the whole column became less dense than before. The water masses in the Lofoten Basin became less dense a couple of years after the Norwegian Basin and the Greenland Sea. From 1985, roughly the whole water column had lighter water masses than before.

As the results show a decrease in density in all basins, the following paragraphs describes how the different density classes have changed in volume. The density classes are ranging from 20 to 28.4 kg/m^3 with increments of 0.01 kg/m^3, and each density class is defined as intervals from $28.01 - 28.02, 28.03 - 28.04,$ etc. The distribution compares the classes and helps to highlight which densities contain the highest volume. This has been done for each basin, the entire Nordic Seas, and for water masses above and below 850 m. The deepest sill depth of the GSR is 850 m, so this limit distinguishes between potential overflow and deeper water masses.

The volume of each density class (Section 2.2.7) in all basins are shown in Figure 3.9. For each basin the largest volume of denser water masses were observed in the first part of the record (1950–1979). For the following periods (1980–1999 and 2000–2018) the distributions shifted such that lighter waters were more voluminous. The resulting volume percentages for each basin are shown in Table 3.1. All basins had the highest volume within the 28.09 kg/m^3 density class ($28.09 - 28.1$) in the first period (1950–1979), except for the Iceland Sea, which had the biggest volume in the 28.08 kg/m^3 class. For the middle period (1980–1999), the density class of 28.08 kg/m^3 contained the highest volume in all of the basins. For the last period (2000–2018) the basins had different density classes dominating the volume. Here the Greenland Sea had 28.06 kg/m^3, the Norwegian Basin had 28.08 kg/m^3, while the Iceland Sea and Lofoten Basin had 28.07 kg/m^3.

(a)

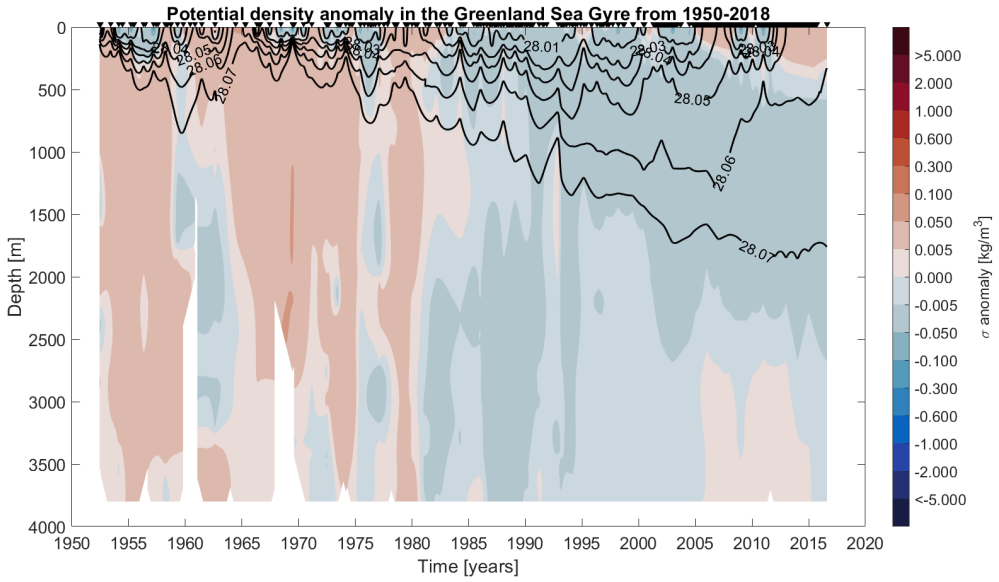

(b)

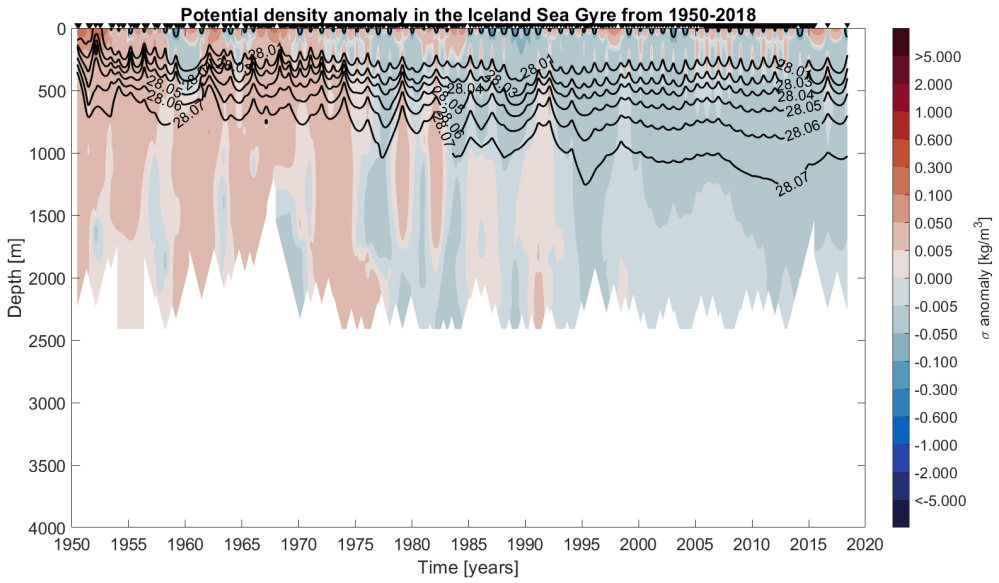

Figure 3.7: Potential density anomalies in the Greenland Sea (a) and Iceland Sea (b) from 1950 to 2018. Red color is density increase, while blue color is density decrease compared to the average profile. The black triangles represents the profiles in the basins. The black lines are the 27.8, 28.01, and $28.03 - 28.07$ kg/m^3 isopycnals.

(a)

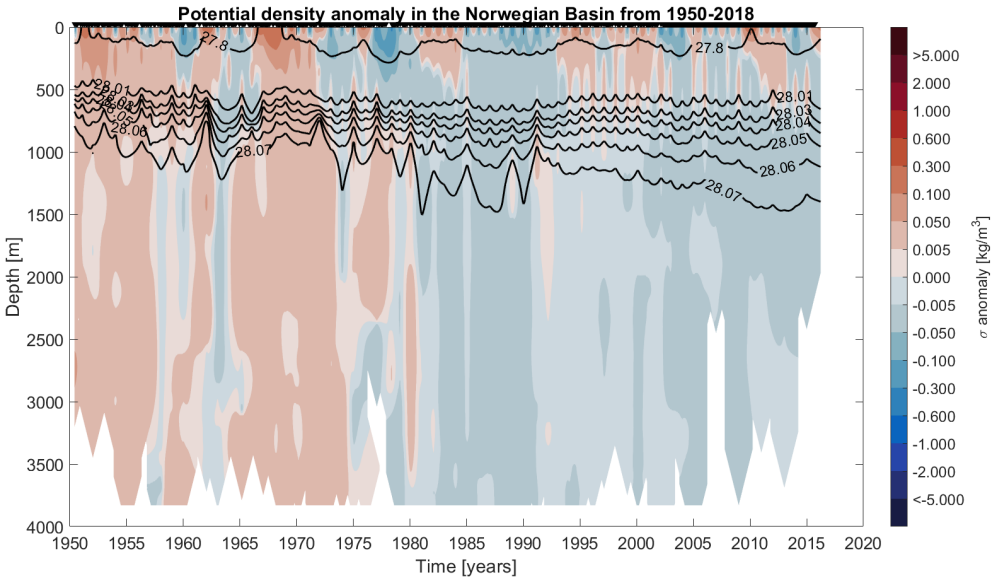

(b)

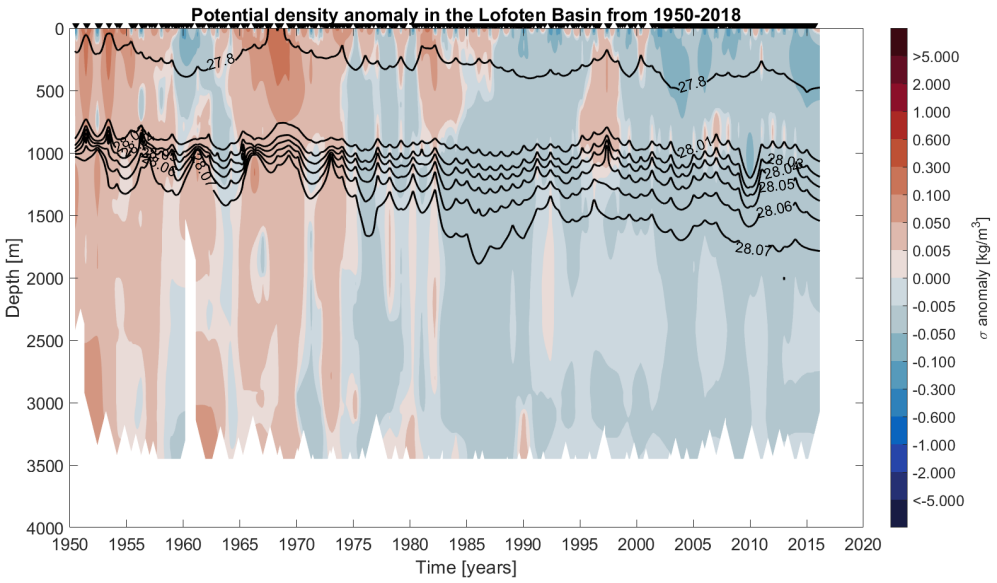

Figure 3.8: As for Figure 3.7, but only for the Norwegian (a) and Lofoten Basins (b).

Table 3.1: The density classes with the highest volume in each basin for the three periods. The numbers are in [%], while the second row includes density classes with unit [kg/m^3]. The largest volumes in each period are marked with bold font. The abbreviations for the basins are: GS = Greenland Sea; IS = Iceland Sea; NB = Norwegian Basin; LB = Lofoten Basin.

	Density classes											
	28.00	**28.01**	**28.02**	**28.03**	**28.04**	**28.05**	**28.06**	**28.07**	**28.08**	**28.09**	**28.10**	**28.11**
Basin	**1950 - 1979**											
GS	0.4	0.7	1.0	1.9	3.5	6.7	11.3	17.6	18.4	**22.3**	10.5	2.2
IS	1.4	1.7	2.0	3.3	5.2	7.6	9.1	15.8	**20.2**	16.3	4.2	1.6
NB	1.4	1.6	2.1	2.8	3.7	5.1	8.7	10.2	14.2	**17.7**	8.7	2.3
LB	1.2	1.3	1.5	1.5	2.2	2.5	4.1	8.2	13.5	**17.1**	7.2	1.6
	1980 - 1999											
GS	0.5	0.7	1.0	1.7	3.2	6.1	12.0	23.2	**46.3**	2.3	0.0	0.0
IS	2.9	3.3	4.5	5.8	7.5	8.9	11.0	12.3	**20.6**	5.5	0.5	0.7
NB	1.6	1.9	2.2	2.4	3.2	4.9	7.3	11.6	**28.1**	12.9	2.1	0.5
LS	1.1	1.3	1.6	2.1	2.8	4.2	5.3	10.0	**27.4**	9.5	2.8	0.1
	2000 - 2018											
GS	0.3	0.5	0.9	1.7	3.2	10.6	**33.4**	15.5	17.0	14.7	0.0	0.0
IS	1.8	2.2	4.5	7.0	8.8	10.8	17.2	**22.7**	13.6	0.0	0.0	0.0
NB	1.9	2.4	3.2	4.2	5.6	7.8	10.5	17.7	**19.9**	2.7	0.0	0.0
LB	1.6	2.0	2.6	3.5	4.8	7.1	10.2	**14.5**	10.0	0.8	0.0	0.0

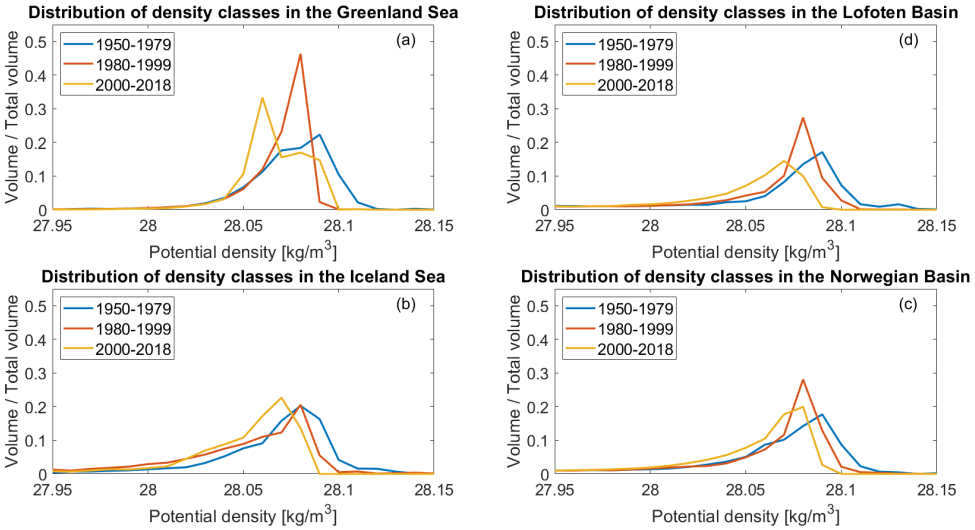

Figure 3.9: Distribution of density classes in the Greenland Sea (a), the Iceland Sea (b), the Norwegian Basin (c), and the Lofoten Basin (d). The blue line is the period 1950–1979, the red line 1980–1999, and the yellow line is 2000–2018.

The density class distribution for the entire Nordic Seas showed a similar shift toward lighter water masses for the different periods (Figure 3.10). The first period (1950–1979) had the highest contributions from 28.08 and 28.09 kg/m^3 with 12.7% and 14.4%, respectively. The densities of 28.07 and 28.08 kg/m^3 occupied most of the volume in the second period (1980–1999), with 12.8% and 23.8%. The last period (2000–2018) had a much more even top in the distribution. Each of the density classes in the range 28.06 – 28.08 kg/m^3 were found in roughly 14% of the total volume. This change in distribution of density classes implies that the water masses of the Nordic Seas have become lighter over the past 70 years.

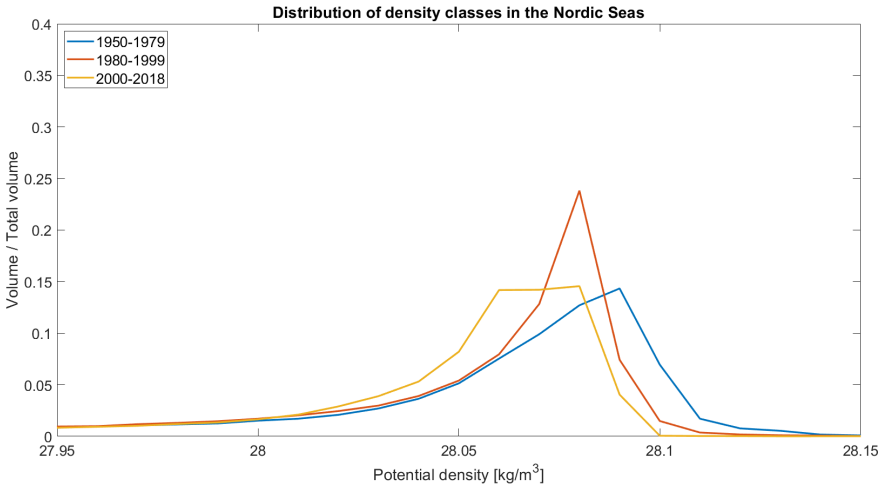

Figure 3.10: Distribution of density classes in the Nordic Seas. The blue line represents the period 1950-1979, the red line is 1980-1999, and the yellow line is 2000-2018.

Splitting the Nordic Seas into two parts, above and below 850 m depth (Figure 3.11), helps to quantify changes in the potential overflow waters and the deeper water masses. The main difference between these two cases is that the water masses above sill depth (850 m) are much less dense than the ones below. The water masses below 850 m also occupy a much larger volume compared to the water masses above 850 m.

The dominating density classes for the water masses above sill depth in the first period (1950–1979) were 28.05 – 28.07 kg/m^3 with 6.4%, 6.8%, and 5.4%, respectively. For the middle period (1980–1999), the 28.04 and 28.05 kg/m^3 density classes were the most voluminous. Those densities occupied 6.5% and 7.1% of the total volume above sill depth. The same density classes were found in most of the volume also in the third period (2000–2018).

The water masses with densities of 28.04 and 28.05 kg/m^3 then covered 8.6% and 10.6% of the total volume.

The water masses below 850 meters showed the same pattern as all of the basins and the entire Nordic Seas. The first period (1950–1979) had highest contributions from 28.08 and 28.09 kg/m^3 with percentages of 21.4% and 26.8%. The middle period (1980–1999) contained less dense water masses, where the 28.07 and 28.08 kg/m^3 had 21.0% and 42.4% of the total volume. The last period (2000–2018) shifted toward lighter density classes. Densities of 28.06–28.08 kg/m^3 occupied 20.4%, 28.9%, and 29.9% of the total volume.

Figure 3.11: Distribution of density classes in the Nordic Seas above (a) and below (b) the deepest sill depth of the GSR (850 m). The blue line is the period 1950–1979, the red line is 1980–1999, and the yellow line is 2000–2018.

3.2 Changes in the hydrographic properties of the NIJ and IFSJ

In this section will changes in depth of the 28.05 kg/m^3 isopycnal and density of the NIJ transport mode be investigated. In addition will also the hydrographic properties along the Icelandic slope and IFR be described. Changes in the hydrography of the NIJ and IFSJ might be related to changes in the Greenland Sea, and therefore be traced back there (Section 1.6).

3.2.1 Isopycnal depth

The shallowest depths of the 28.05 kg/m^3 isopycnal were found in the Greenland Sea in both of the two periods (1980–1999 and 2000–2018; Figure 3.12). This is mainly because of the dense water formation in the Greenland Sea.

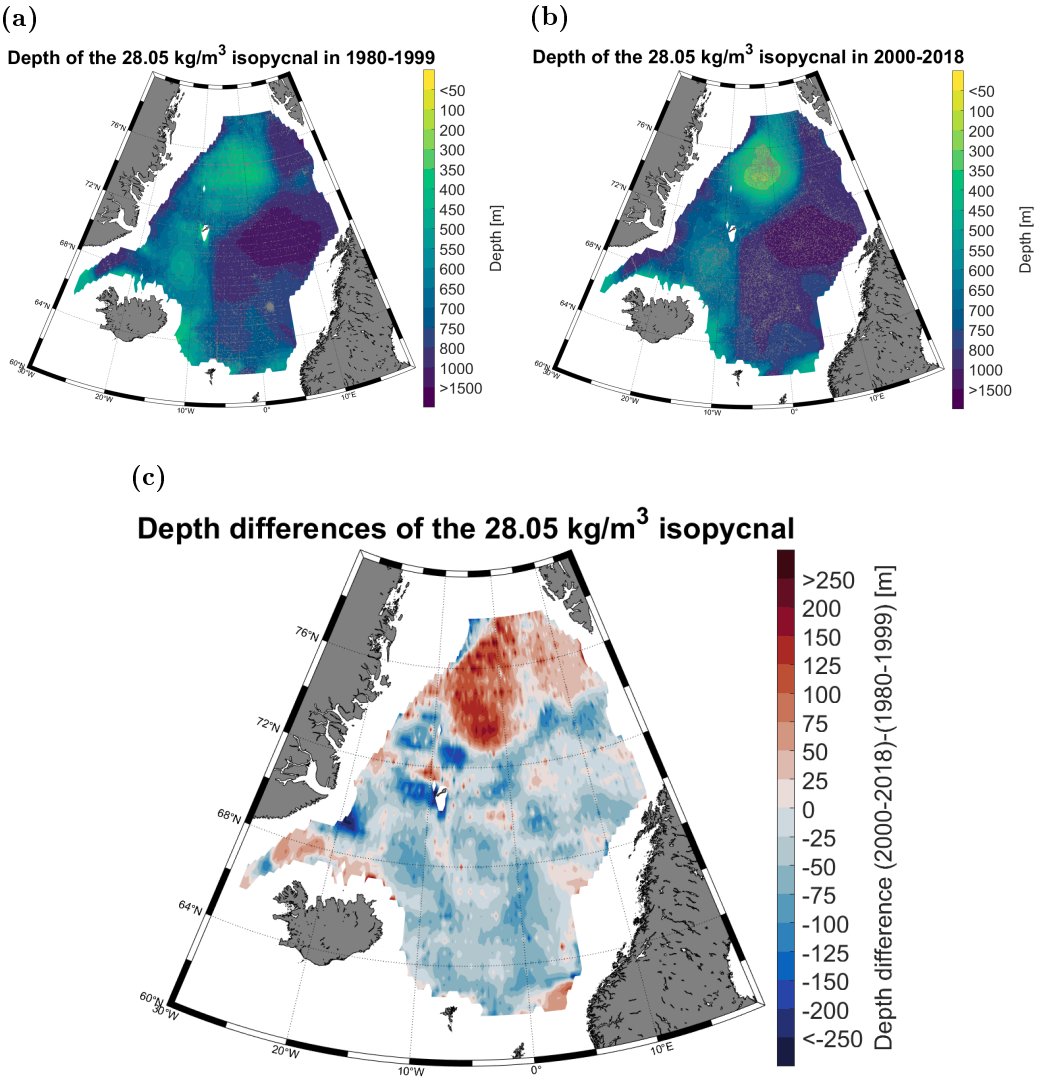

Figure 3.12: Depth of the 28.05 kg/m^3 isopycnal in the Nordic Seas in 1980–1999 (a), 2000–2018 (b) and difference between the two periods (c). The record contains profiles for all months. The grey dots (a-b) show the locations of the profiles. In (c), the blue color is a deepening of the isopycnal, while red shows that the isopycnal is higher in the water column than before.

Convection are extending to greater depths and the water column densifies, which increases the density in the entire water column and dense water masses are located at shallower depths in the Greenland Sea. The difference between the two periods (Figure 3.12c) showed that the 28.05 kg/m^3 isopycnal deepened from the first to the last period in most of the Nordic Seas, except for the Greenland Sea. Here the isopycnal shoaled and was found higher in the water column compared to earlier. This was mainly due to the formation of the new class of GSAIW (Brakstad et al., 2019).

A more detailed evolution of the 28.05 kg/m^3 isopycnal depth in each of the basins will described in the upcoming paragraphs. This was done to identify how and when the depth changed.

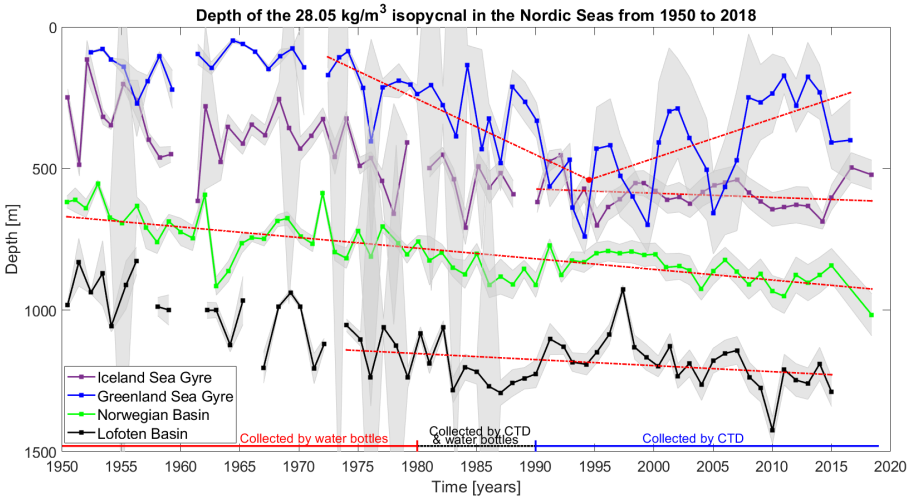

Figure 3.13: Time series of the depth of the 28.05 kg/m^3 isopycnal in the four basins from 1950 to 2018. The grey shading shows the standard deviation, while the red dashed line indicates linear trends. The red points mark breakpoints (Section 2.2.4).

The isopycnal deepened in the Greenland Sea by –200±120 m/decade until 1994. In 1994 the isopycnal trend changed from a deepening to a shoaling. After 1994 the depth of the isopycnal became shallower at a rate of $+137 \pm 23$ m/decade. This change took place at the same time as the formation of the new class of GSAIW started, which was documented by Brakstad et al. (2019). The stratification in the Greenland Sea weakened due to an increase in the near-surface salinity in 1993. From this weakening in stratification together with strong atmospheric forcing, convection in the Greenland Sea exceeded 500 m and the formation of the new class of GSAIW started.

While the isopycnal was found at shallower depths in the Greenland Sea after 1994, the remaining basins continued to have a deepening rate. The isopycnal in the Norwegian and Lofoten Basins deepened with rates of -38 ± 8 m/decade and -21 ± 46 m/decade, respectively. The isopycnal in the Iceland Sea deepened from 1990 to 2018 at -15 ± 6 m/decade.

3.2.2 The transport mode of the NIJ

The NIJ transport mode represents the average hydrographic properties of the bulk of the water masses transported by the NIJ (Section 1.4.1). By summation of profiles at depth intervals of 100 m from different stations along the Icelandic slope, an average estimate (with errors) of temperature and salinity is obtained (Semper et al., 2019). This study uses three stations (KG5, SI8 and SL5) when calculating the NIJ transport mode (Figure 3.14). These stations represents the NIJ well because of the similar values of temperature and salinity (Figure 3.17).

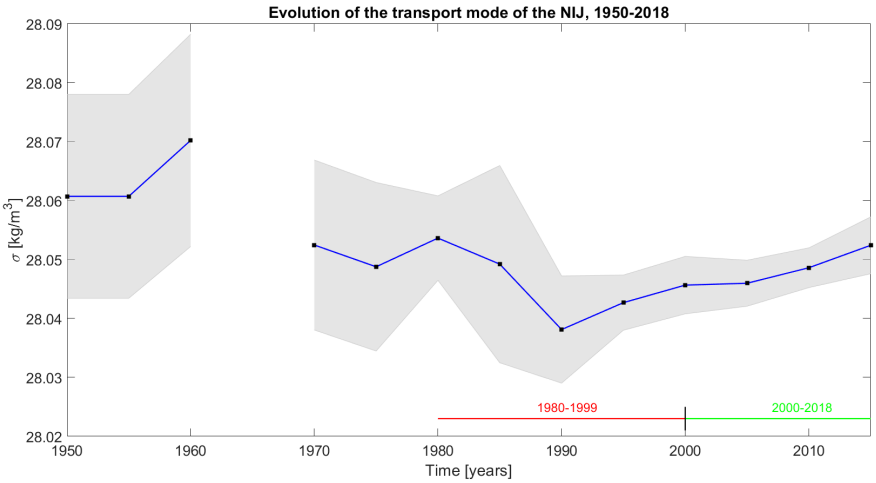

Figure 3.14: 5-year means of the density of the NIJ transport mode. The grey shading shows the standard deviation.

The density of the NIJ transport mode decrease from 1960 to 1990 and increased from 1990 to 2015. This corresponds well with the change from production of GDSW to the new class of GSAIW. Overall the NIJ transport mode was located in a range from 28.04 to 28.07 kg/m^3.

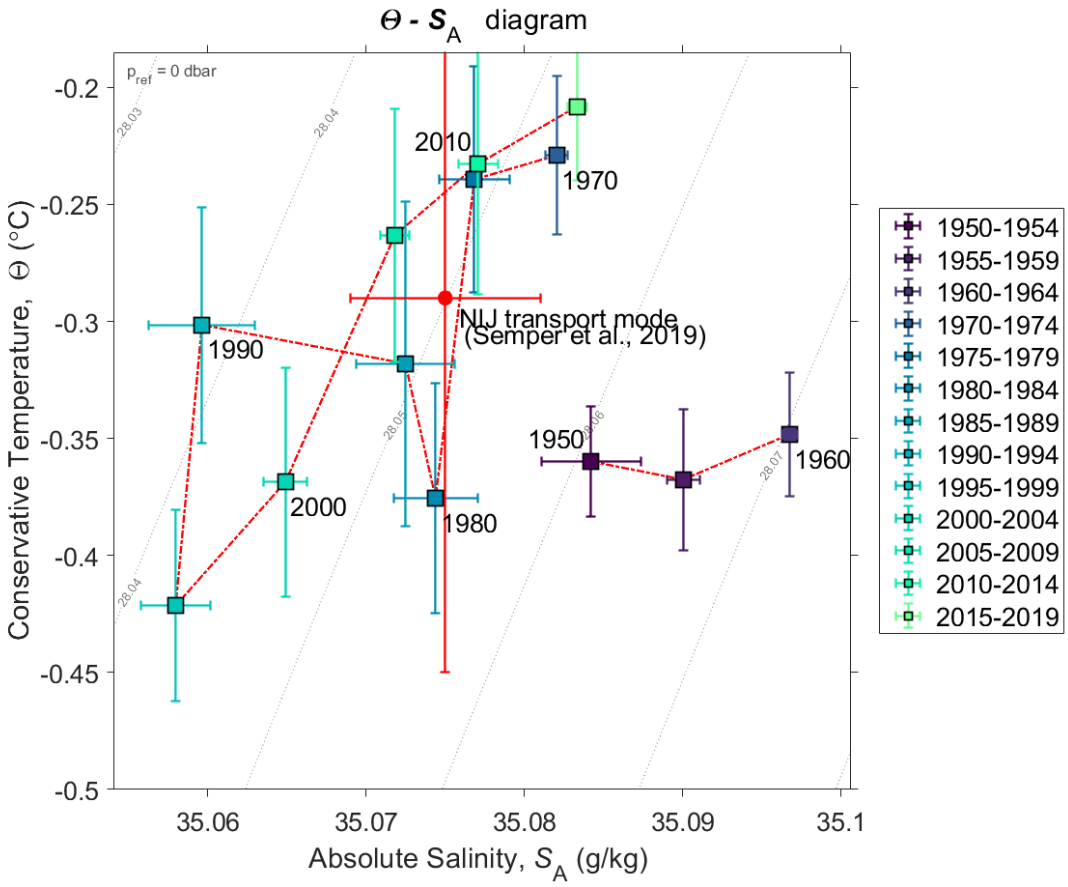

Figure 3.15: θ – S diagram showing the transport mode of the NIJ. Each value represents a 5-year average. The red point is the NIJ transport mode defined by Semper et al. (2019).

The time series of the NIJ transport mode (Figure 3.14) has been plotted in a θ–S diagram with the respective conservative temperature and absolute salinity values for each 5-year period. The early values (1950–1964) are denser than the transport mode of 28.05 kg/m^3 defined by Semper et al. (2019). From 1970 to 1979, the transport mode was located around 28.05 kg/m^3, with higher temperatures than the transport mode defined by Semper et al. (2019). Thereafter the values became colder, less dense and less saline, before they increased in salinity and density again from 1990. Apart from the beginning of the record (1950–1965) and 1990–1994, the transport mode was within a range of 28.04 to 28.06 kg/m^3. Semper et al. (2019) based the value of the NIJ transport mode on data from 2004 to 2018, with a value of 28.05 ± 0.01 kg/m^3. The overall average transport mode from this study is 28.05 ± 0.005 kg/m^3.

3.2.3 Changes in hydrographic properties of the NIJ and IFSJ

This section describes how the water masses transported by the NIJ and IFSJ have changed over time. Each of the stations show resulting changes within a depth interval where the 28.05 kg/m^3 isopycnal are found. The different depth intervals for the stations can be found in the legend in Figure 3.17. As the IFSJ is located deeper than the NIJ, I considered an interval from 1000 to 1200 m on Station 5 (Section 1.4.2).

The temperature of the water masses at the NIJ stations increased during the 1990s by an average rate of 0.08 ± 0.06°C/decade (Figure 3.16). Water masses at Station 5, covering the IFSJ, warmed by a similar magnitude (0.06 ± 0.03°C/decade).

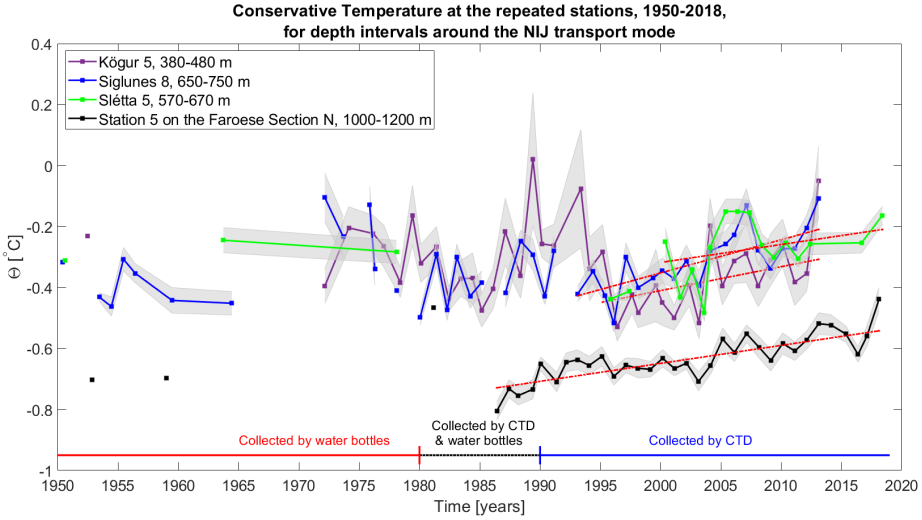

Figure 3.16: Temperature time series from 1950 to 2018 at stations in the NIJ and IFSJ. Each line represents the depth intervals at the stations. The grey shading shows the standard deviation. The red dashed lines indicate linear trends, while the red points mark the breakpoints (Section 2.2.4). For station locations see Figure 2.2.

As the temperature increased, the salinity increased as well. The water masses at the NIJ stations became more saline from around the mid–1990s (Figure 3.17a). The average increase in salinity was $(1.53 \pm 0.23) * 10^{-2}$ g/kg per decade. The density at station 5 had first a period from 1986 to 1997 where the salinity decreased, before the water masses became more saline after 1997. These changes also affected the density evolution.

(a)

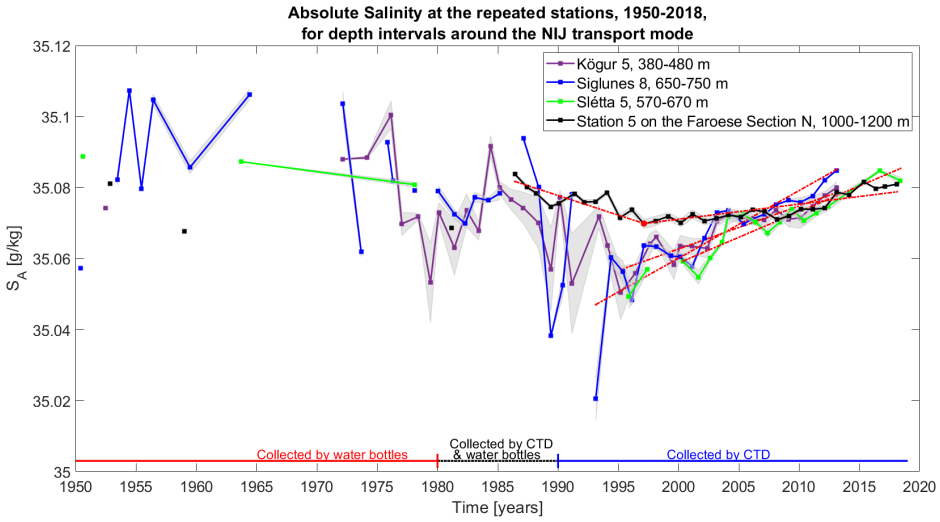

(b)

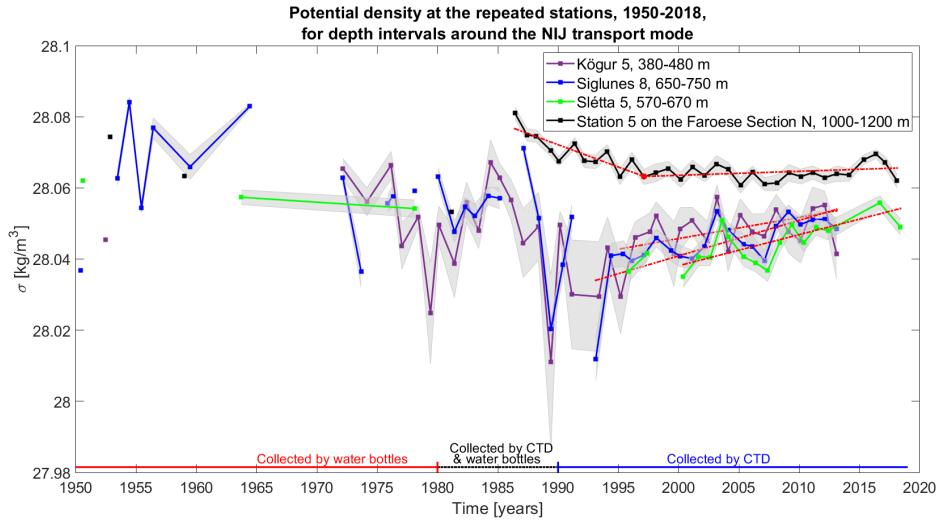

Figure 3.17: As for Figure 3.16, just for salinity (a) and density (b).

From the mid–1990s, the water masses of the NIJ increased in density, by an average rate of $(8.3 \pm 5.7) * 10^{-3}$ kg/m^3 per decade. Stations 5, on the other hand, decreased in density from 1985, before increasing from around 1997 at a slower rate than the NIJ stations.

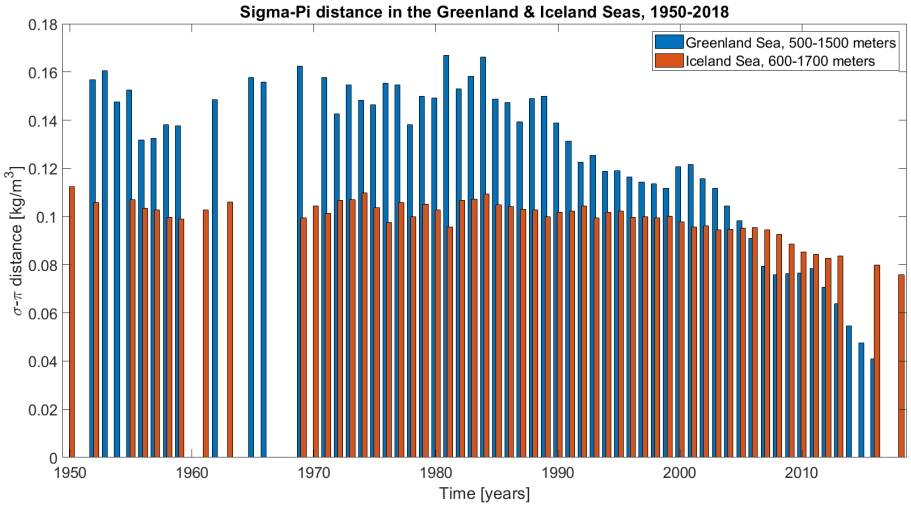

Figure 3.18: Changes of σ–π distance between water masses in the Greenland and Iceland Seas and the transport mode of the NIJ (Semper et al., 2019) from 1950 to 2018. The blue bars represent the Greenland Sea (500–1500 m), while the red bars show the Iceland Sea (600–1700 m).

The $\sigma - \pi$ distance in Figure 3.18 is the distance between water masses in the Greenland and Iceland Seas, and the transport mode of the NIJ (Section 2.2.2; Semper et al., 2019). The depth interval 600–1700 m (Iceland Sea) was chosen from the corresponding density range in the mixed layer in the Greenland Sea (500–1500 m; Section 2.2.4). These distances are calculated to examine which of the two basins have the water masses that are most similar to the transport mode. Since the western part of the Nordic Seas (especially the Greenland Sea) is hypothesized to the be source of the densest overflow waters, these basins are of particular interest (Huang et al., in review).

In the beginning of the record, the distance between the properties of the NIJ transport mode and the properties of the water masses in the Greenland Sea was relatively high. From around 1985, the distance started to decrease. After 2000 the distances decreased more rapidly and the properties of the water masses in the Greenland Sea became closer to the properties of the transport mode. The Iceland Sea showed a more constant signal, where the distance first decreased in 2005.

By averaging over the record the Greenland Sea has the lowest $\sigma - \pi$ distances, and the water masses here were closer to the properties of the NIJ transport mode.

3.2.4 Sources of overflow water

As mentioned in the previous section, the $\sigma - \pi$ distance between the water masses in the Greenland and Iceland Sea gyres, and the transport mode of the NIJ are of particular interest. This is because the Greenland Sea is hypothesized to be a main source of the overflows, with transport of dense water southwards into the Iceland Sea along the Jan Mayen and Kolbeinsey ridges (Huang et al., in review). As the lowest $\sigma - \pi$ distances are found in the Iceland and Greenland Seas (Huang et al., in review), we further investigated changes in the vertical distribution of this distance (Figure 3.19).

In the period from 1950 to 1990 the lowest $\sigma - \pi$ distances were found near 500 m in the Greenland Sea Gyre (Figure 3.19a). From 1990 the $\sigma - \pi$ distance began to decrease in the entire water column. The lowest values were found between 500 and 1500 m for the rest of the period. This fits very well with formation of GSAIW (Brakstad et al., 2019).

The $\sigma - \pi$ distance in the Iceland Sea Gyre remained constant in the entire water column for the whole period. The lowest values were found in the layer between 300 and 700 meters.

(a)

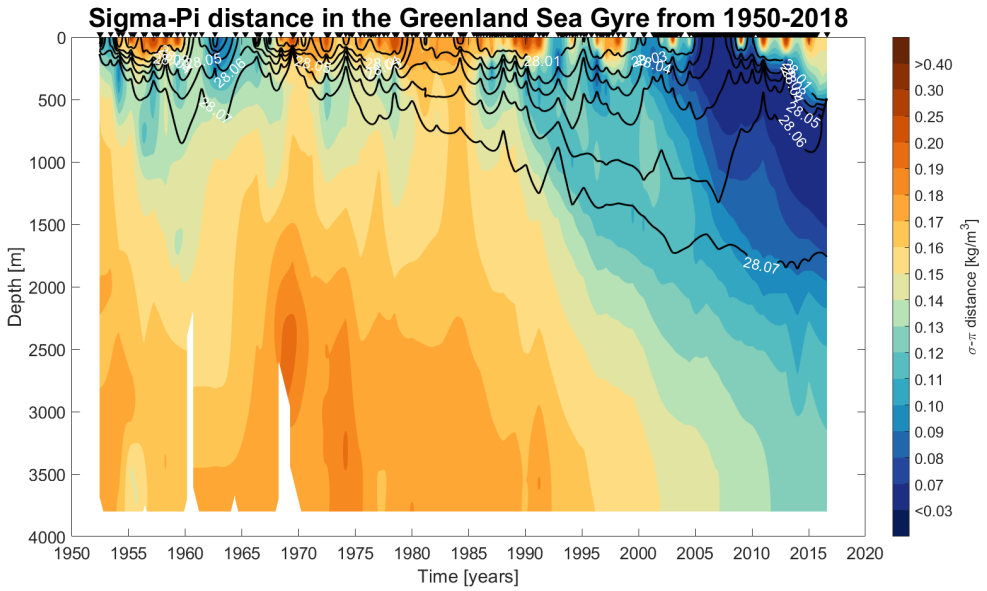

(b)

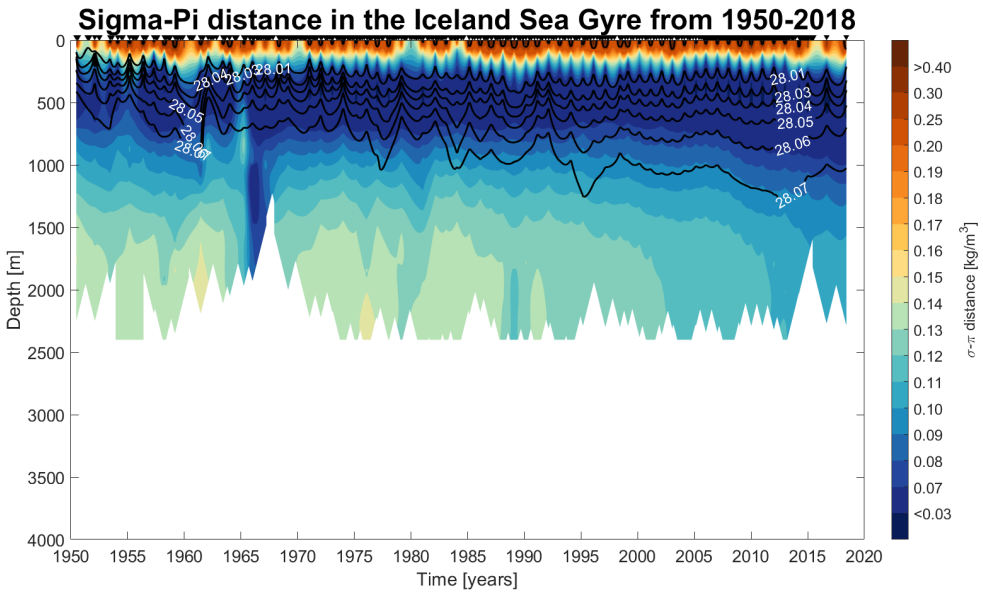

Figure 3.19: $\sigma - \pi$ distance in the Greenland Sea (a) and the Iceland Sea (b) from 1950 to 2018. The distance are calculated between the water masses in the Greenland and Iceland Seas and the transport mode of the NIJ (Semper et al., 2019). The black lines are the 28.03 – 28.07 kg/m^3 isopycnals. The black triangles represents the time of the profiles.

3.2.5 Changes in hydrography along the Icelandic slope and the Iceland-Faroe Ridge

Average temperatures and salinities over the entire period (1950–2018) along the Icelandic slope and IFR were obtained from the interval of 28.04 – 28.06 kg/m^3 (the band defined in Section 2.2.3). This interval covers the range of the transport mode of the NIJ. The highest temperatures are located near Denmark Strait (Figure 3.20a). There is also a warmer area in the northern part of the band, north of Iceland. The reason for this warming signal north of Iceland is the influence of the warmer and more saline Atlantic-Origin water transported by the EGC. For the rest of the area east of Iceland, the temperature was constant.

Salinity shows a similar pattern as temperature (Figure 3.20c), with saline water masses around Denmark Strait and north of Iceland. The remaining areas show a salinity with little spatial variability.

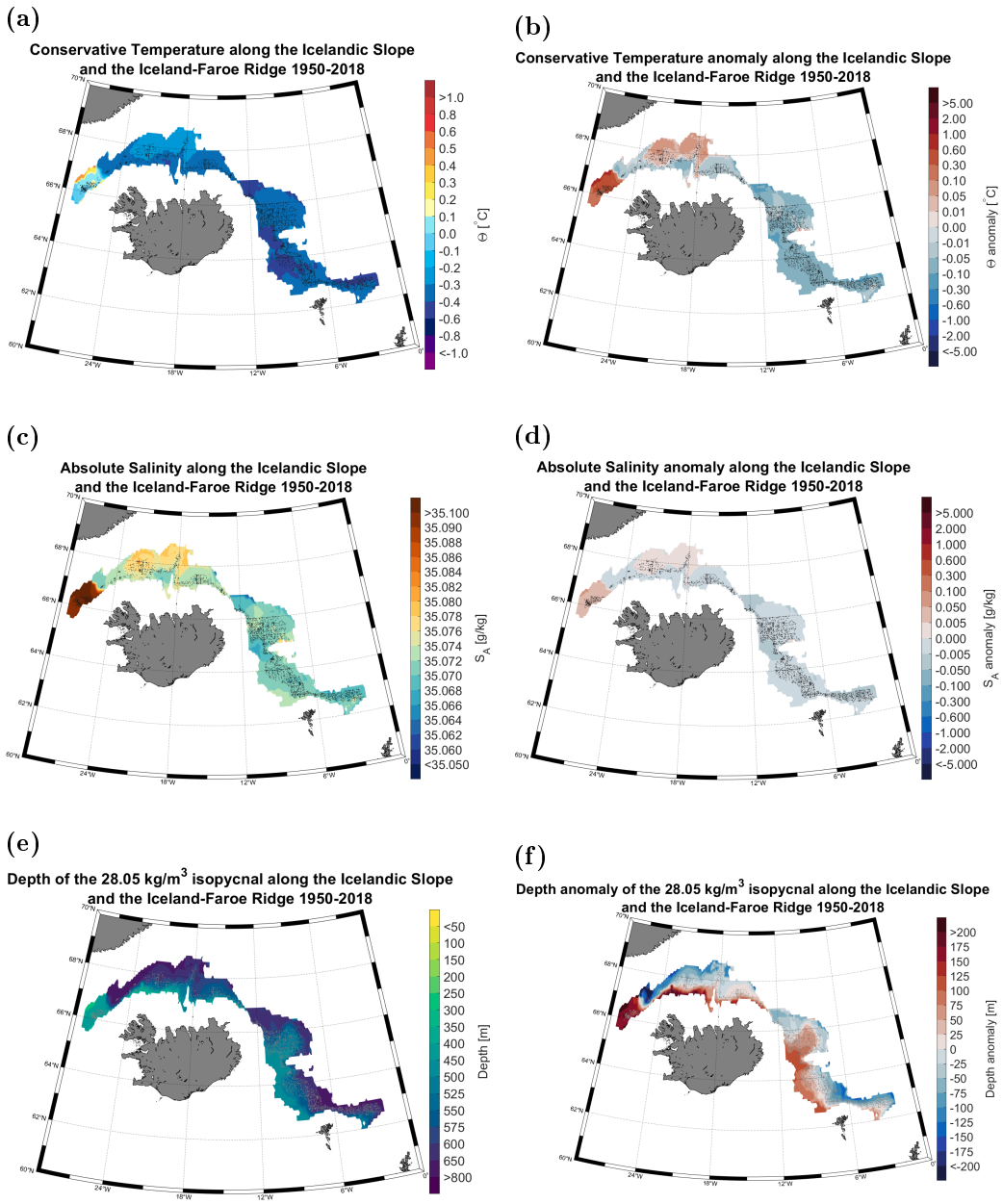

Figure 3.20: Temperature (a-b), salinity (c-d) and depth of the 28.05kg/m^3 isopycnal (e-f) along the Icelandic slope and IFR from 1950 to 2018. The right panels show anomalies relative to the average of the entire area. For the anomalies the red color indicate an increase, while the blue color is a decrease. In (f), blue values indicate a deepening, while red show a shoaling of the 28.05 kg/m^3 isopycnal.

The 28.05 kg/m^3 isopycnal is found at shallow depths in Denmark Strait and along the Icelandic slope. The farther away from the continental slope, the deeper the isopycnal is located. Along the Icelandic slope and all the way to the Faroe Islands, the isopycnal shows signs of upbanking of dense water towards the slope. This is typical signatures for both the IFSJ (Semper et al., in review) and NIJ (Pickart et al., 2017). The anomalies (Figure 3.20f) also indicate increased upbanking towards the slope, where positive values indicate a shoaling of the isopycnal depth compared to the average value.

In this part of the section will the vertical section along the band (Section 2.2.3) be investigated. Near Denmark Strait and the Faroe Islands warmer temperatures extended deeper into the water column (Figure 3.21a) This is related to inflows of Atlantic and Irminger Water. The warm waters from the Faroe Branch of the inflow were also shown in the top right corner in Figure 3.21a. Along the Icelandic slope until 1000 km from Denmark Strait, the warmer temperature only extended down to roughly 250 m depth. The IFSJ also transported colder water masses than the NIJ. For the NIJ, the temperature between 600 and 850 m depth was roughly between 0 and –0.6°C. The water masses of the IFSJ were colder, ranging from –0.4 to colder than –0.8°C. This is expected as the IFSJ is a bottom-intensified current.

The upper 500 m contained fresh water masses, with saltier waters below. From 1100 to 1500 km very saline water masses were present in the upper 500 m. This is inflowing Atlantic Water, which is warm and saline. Both the NIJ and IFSJ have water of the same salinity, which can also be confirmed by their transport modes (Sections 1.4.1 and 1.4.2).

Closer to both Denmark Strait and the FBC, the isopycnals were sloping downwards (Figure 3.21c). Along the Iceland slope and the IFR the isopycnals were fairly flat. The density of the NIJ ranged mainly from 28.03 to 28.06 kg/m^3, in the depth interval from 600 to 800 m. The IFSJ showed a denser signature, with densities greater than 28.05 kg/m^3 in the depth interval from 750 to 1100 m. These intervals are the isobaths were the cores of the currents are located.

The main findings from this analysis are the sloping isopycnals close to both Denmark Strait and the FBC. Comparing the properties of the IFSJ and NIJ show that they carry water masses with similar hydrographic properties.

(a)

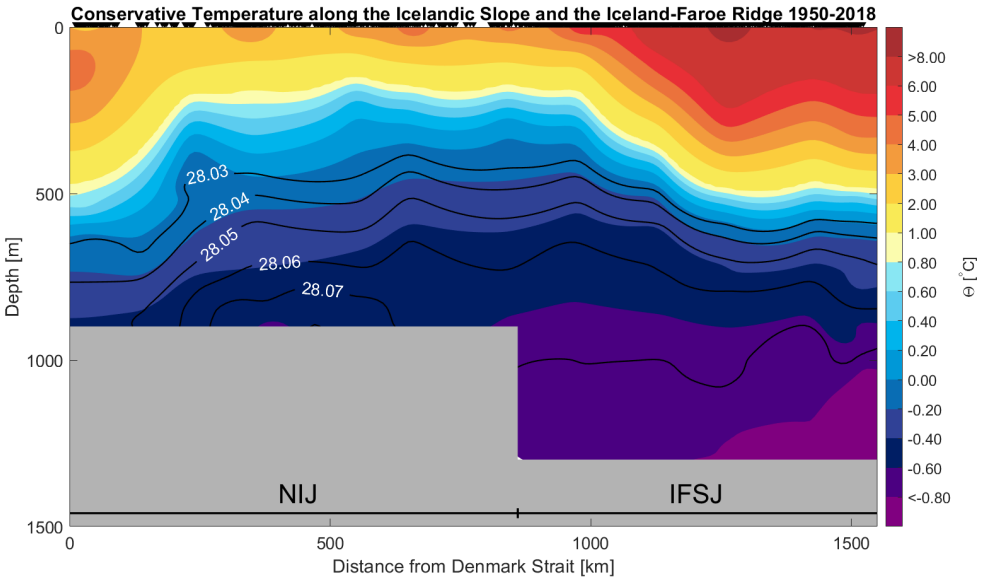
Conservative Temperature along the Icelandic Slope and the Iceland-Faroe Ridge 1950-2018
Depth [m]
0
500
1000
1500
28.03
28.04
28.05
28.06
28.07
NIJ
IFSJ
0
500
1000
1500
Distance from Denmark Strait [km]
>8.00
6.00
5.00
4.00
3.00
2.00
1.00
0.80
0.60
0.40
0.20
0.00
-0.20
-0.40
-0.60
<-0.80
Θ [°C]

(b)

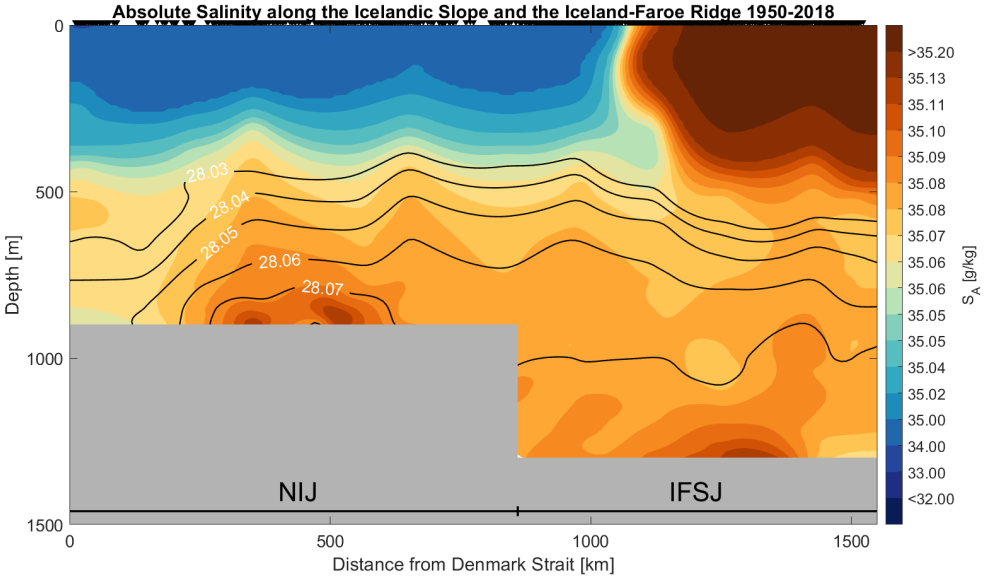
Absolute Salinity along the Icelandic Slope and the Iceland-Faroe Ridge 1950-2018
Depth [m]
0
500
1000
1500
28.03
28.04
28.05
28.06
28.07
NIJ
IFSJ
0
500
1000
1500
Distance from Denmark Strait [km]
>35.20
35.13
35.11
35.10
35.09
35.08
35.08
35.07
35.06
35.06
35.05
35.05
35.04
35.02
35.00
34.00
33.00
<32.00
S_A [g/kg]

(c)

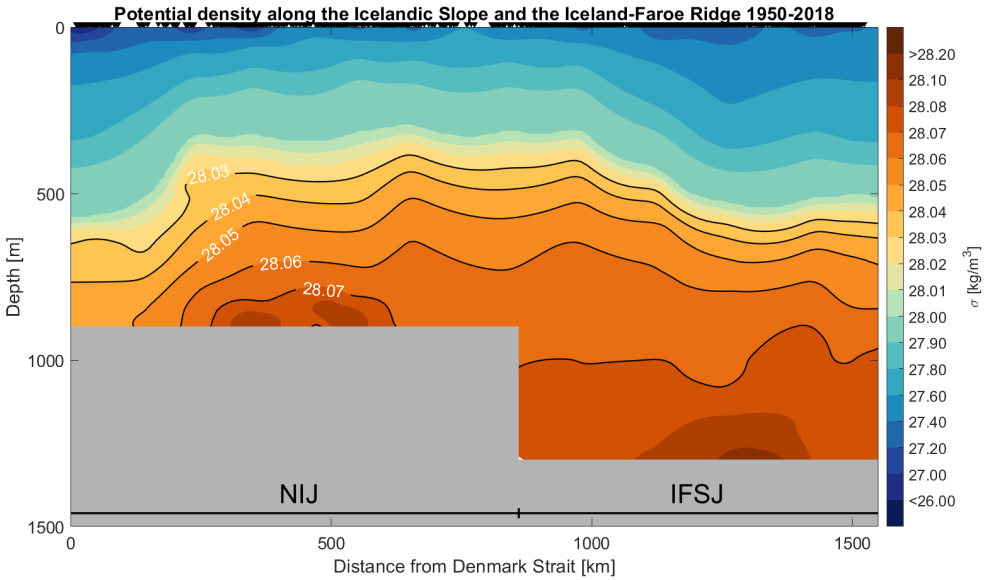

Figure 3.21: Temperature (a), salinity (b), and potential density (c) sections along the band from Denmark Strait to the Faroe Islands. The black lines outline the 28.03 – 28.07 kg/m^3 isopycnals. The grey boxes indicate the bathymetry (900 m for the NIJ and 1300 m for the IFSJ).

Chapter 4

Discussion

4.1 Hydrographic changes in the Nordic Seas

4.1.1 Reduced convection in the Greenland Sea

Bottom convection in the Greenland Sea ceased in the beginning of the 1980s. Before 1980 the convection extended almost to the bottom (Aagaard and Carmack, 1989; Carmack and Aagaard, 1973). Production of cold and dense GSDW occurred during winter, and this dense water mass prevented warm and less dense water masses from entering the Greenland Sea. After 1980, convection in the Greenland Sea was limited to intermediate waters (Meincke et al., 1997). When lighter water masses from the EGC entered the Greenland Sea, a warming started. This warming trend in the Greenland Sea was also documented in previous publications (Lauvset et al., 2018; Wang et al., 2015; Østerhus and Gammelsrød, 1999). Lauvset et al. (2018) observed temperature rates corresponding to 0.21°C/decade at 1000 m and 0.16°C/decade at 1500 m. Wang et al. (2015) found a warming that was relative to 0.21°C/decade in the depth interval 1900–2200 m. Both these publications compare well with the temperature rate observed in the depth interval of 500–1500 m (0.21°C/decade). The deep waters (below 2000 m) warmed by 0.14°C/decade, and this result compares well with what Østerhus and Gammelsrød (1999) and Wang et al. (2015) observed. 0.09°C/decade at 3000 m and 0.13°C/decade at 2000 m, were indicated by Wang et al. (2015) and Østerhus and Gammelsrød (1999), respectively.

In the decades following 1980 the Greenland Sea became warmer and more saline due to the convective changes. The temperature and salinity changes from 1980–1999 to 2000–2018 (Figure 3.1) indicated a big change in the water column structure of the Greenland Sea Gyre. This large change

seems to be the main reason for the changes observed also in the rest of the Nordic Seas basins. Lack of convection extending into the deeper parts allowed less dense water masses to enter the Greenland Sea which changed the properties within the gyre. This lack of bottom convection also stopped the production of GSDW, and the water masses transported out of the Greenland Sea were less dense. This altered the other basins with lighter water masses found at shallower depths. Hence, the properties in all basins changed due to the changes in the deeper water masses from the Greenland Sea.

Another reason for the increase in temperature and salinity may be a change in the inflowing waters. If the waters flowing into the Greenland Sea are warmer and more saline now compared to earlier years, the properties will change (Lauvset et al., 2018). There has always been some inflow of warmer water into the Greenland Sea, but after the bottom convection ceased in the 1980s, more of these water masses have mixed with the ambient water masses in the Greenland Sea. The mixed water masses will have a higher salinity and temperature than the original water masses within the gyre. With warmer and more saline water masses in the gyre, the exchange from the Greenland Sea will contain less dense water and the other basins will be impacted by this change.

4.1.2 The Nordic Seas are connected

The Greenland Sea is most likely the source of the warming trend appearing in the beginning of the 1980s. The density of the typical mixed layer in the Greenland Sea was used to define the depth intervals in the other basins (Figure 3.2). The breakpoints indicate where the change in the trend is largest. Therefore, the location of these breakpoint is important when determining when the warming started in the basins. When the Greenland Sea first started to warm in the beginning of the 1980s, the other basins showed a warming roughly 10 years after the Greenland Sea. Therefore, is it likely that the changes in the Greenland Sea impacted the other basins.

A warming trend in the Norwegian Sea was also documented by Mork et al. (2019), Wang et al. (2015), and Østerhus and Gammelsrød (1999). The temperature rate observed in the Norwegian Basin was 0.05°C/decade, in a depth interval from 750 to 1750 m. Mork et al. (2019) documented a warming rate of 0.046°C/year which is relative to 0.46°C/decade for the upper 1000 m. Wang et al. (2015) estimated a total warming at 2000 m in the period 1984–2012, which corresponds to a warming of 0.05°C/decade. Østerhus and Gammelsrød (1999) found a warming rate at 2000 m, that corresponds to 0.09°C/decade. Mork et al. (2019) had a much higher rate compared to this thesis, but that is mainly due to consideration of different

depth intervals. The temperature increase is much more similar to the rates found by Wang et al. (2015) and Østerhus and Gammelsrød (1999). The Lofoten Basin warmed by similar temperature rate as the Norwegian Basin. This compares well with Wang et al. (2015) which documented a temperature rate corresponding to 0.07°C/ decade. Mork et al. (2019) found a warming of 0.51°C/year in the upper 1000 m from 2011 to 2018, but they considered a different depth interval than this thesis.

Jeansson et al. (2017) showed that the intermediate water masses between 200 and 400 m depth in the Iceland Sea had similar rates of change in temperature and salinity as the Greenland Sea from the beginning of the 2000s. They suggested that the water masses had propagated from the Greenland Sea into the Iceland Sea. Jeansson et al. (2017) also found that intermediate water masses from both the Greenland and Iceland Seas were important for the intermediate water masses in the Norwegian Sea, but at different densities. This indicates that the advection of water masses between the basins occurred isopycnally.

The densest water masses in the Iceland Sea are likely to originate from the Greenland Sea. Some water masses are also produced locally, but not the densest ones (Våge et al., 2015). Huang et al. (in review) hypothesized that the dense water masses were transported southwards from the Greenland Sea, into the Iceland Sea along the Kolbeinsey and Jan Mayen ridges. The warming signal in the Iceland Sea (Figure 3.4b) can therefore be traced back to the Greenland Sea. Mork et al. (2014) documented an exchange across the Jan Mayen Ridge of warm and saline waters from the Norwegian Sea towards the Iceland Sea. The findings from both Mork et al. (2014) and Jeansson et al. (2017) indicate an exchange in both directions between the Iceland and Norwegian Seas.

For the two basins in the Norwegian Sea a warming signal was observed in the mid–1990s. Dense water masses from the Greenland Sea are transported through the Jan Mayen Channel into the Norwegian Sea. These water masses reach the Norwegian Basin first, before flowing northwards into the Lofoten Basin. There is also a more direct exchange between the Greenland Sea and the Lofoten Basin across the Mohn Ridge (Spall, 2010).

The Greenland Sea plays an important role in the Nordic Seas by producing dense water, but also as a source of the hydrographic changes. The warming signal first discovered in the Greenland Sea was observed later in the other basins because the water masses from the Greenland Sea spread out to the other basins. The result has been a significant change in the entire density distribution in the Nordic Seas.

4.1.3 Structural changes in the Nordic Seas

The density structure in the Nordic Seas has changed since the 1980s. When the production of very dense water masses was shut off around 1980, it impacted the density distribution in the entire Nordic Seas.

Comparing how the volume of density classes has changed from 1950 to 2018 (Figure 3.10) indicates a structural change in the Nordic Seas. The water masses became less dense from 1950–1979 to 2000–2018. The density classes containing most of the total volume shifted towards lower densities. The same pattern was observed in all four basins (Figure 3.9) and for the water masses below and above the deepest sill depth (850 m) of the GSR (Figure 3.11). The density classes that occupied most of the total volume were different in each of the three different periods (1950–1979, 1980–1999, and 2000–2018), changing from $28.08 - 28.09$ kg/m^3 to $28.06 - 28.07$ kg/m^3, indicating a density decrease over time.

The structural changes can be related to the changes in convective activity in the Greenland Sea that started in the 1980s (Østerhus and Gammelsrød, 1999; Meincke et al., 1997). Convection went from ventilating the GSDW to forming a less dense class of GSAIW (Brakstad et al., 2019). As the bottom waters in the Nordic Seas generally contained large proportions of GSDW, the lack of production of GSDW was the major reason for a warming in the deep waters. Østerhus and Gammelsrød (1999) suggest that this warming trend was a result of GSDW being replaced by an increased amount of warmer deep waters from the Arctic Ocean..

Another possible reason for the convective changes in the Greenland Sea and, thus, the structural change in the Nordic Seas can be the retreat of sea ice. In the beginning of the 1980s the sea ice began to retreat towards Greenland (Moore et al., 2015). The highest heat loss is found near the ice edge, and when the sea ice retreated, the distance between the ice edge and the interior gyres increased. This moved the source of heat loss, which weakens the stratification, farther away from the gyres and decreased the likelihood for convection to occur.

Denser water masses were found much deeper in the water column when more of the total volume was occupied by lighter masses. The 28.05 kg/m^3 isopycnal deepened in the entire Nordic Seas (Figure 3.12), except for the Greenland Sea. Since 1994, the 28.05 kg/m^3 isopycnal has been found at shallower depth because of the the formation of the new class of GSAIW. GSAIW was first discovered in the 1970s by Malmberg (1983), but the new class of GSAIW has since 1994 been the main product of convection in the Greenland Sea (Brakstad et al., 2019). From 1994, convection started to exceed 500 meters, and there was produced less GSDW, but bigger amounts of

GSAIW. This supports the results of a shoaling of the 28.05 kg/m^3 isopycnal in the Greenland Sea Gyre after 1994.

4.2 Changes in hydrographic properties in the NIJ and IFSJ

4.2.1 Impact on the overflows

The density of the NIJ transport mode ranges between 28.04 and 28.06 kg/m^3 (Semper et al., 2019). This is the bulk of the dense water that the current transports towards Denmark Strait. Before 1990, the hydrographic properties did not show a significant trend, but in the beginning of the 1990s the temperature, salinity, and density started to increase (Figure 3.17). The density of the NIJ transport mode (Figure 3.14) also decreased until 1990, before the density increased again after 1990.

East of Iceland the IFSJ is transporting dense water towards the FBC (Semper et al., in review). My estimates suggest that the temperature of the IFSJ increased from 1986 until the end of the record, while both the density and salinity decreased from 1986 until the mid-1990s. From the mid-1990s the salinity and density began to increase.

Since the NIJ and IFSJ are transporting similar water masses towards the overflows, it has been suggested that they have the same origin (Huang et al., in review; Semper et al., in review). The Greenland Sea is likely to be the source of the water masses transported by both the NIJ and IFSJ, because substantial amounts of dense water ($\sigma > 28.03$ kg/m^3) are formed there during winter. Hence, changes in the Greenland Sea water masses are most likely the main reason for the changes in temperature and salinity of the NIJ and IFSJ. A change in the water masses in the Greenland Sea is therefore likely be observed at a later time in the NIJ and IFSJ.

The $\sigma - \pi$ distances between the water masses in the Greenland and Iceland Seas and the transport mode of the NIJ (Figure 3.18) quantified how close the water masses in the Greenland and Iceland Seas, and the water masses transported by the NIJ were in properties. The Iceland Sea showed a fairly constant signal, with a small decrease in the middle of the 2000s. The Greenland Sea decreased first around 1985, before a more rapid decrease occurred after 2000. The small $\sigma - \pi$ distances indicate that the origin of the overflow waters is in the western part of the Nordic Seas. In the early period of the record (1950-1990) the origin is likely to be the outside of Greenland Sea Gyre and closer to the Iceland Sea. From 1990 the origin is likely to the Greenland Sea Gyre because of the decrease in $\sigma - \pi$ distance. The decrease in

$\sigma - \pi$ distance is most likely due to the formation of the new class of GSAIW (Brakstad et al., 2019).

4.2.2 Spatial changes in the NIJ and IFSJ

Temperature and salinity along the band from Denmark Strait to the FBC show warm and saline values near Denmark Strait and north of Iceland (Figure 3.20a and Figure 3.20c). Apart from these areas, the hydrographic properties remained constant. These results are as expected with the inflow of the separated EGC. The depth of the 28.05 kg/m^3 isopycnal shows upbanking of dense water along the slope (Figure 3.20f). This is a known pattern for both the IFSJ (Semper et al., in review) and NIJ (Pickart et al., 2017). Closer to both the FBC and Denmark Strait the isopycnals are sloping downwards (Figure 3.21c).

Macrander et al. (2005) demonstrated that Denmark Strait is hydraulically controlled. This was confirmed by requirements, such as a deepening of isopycnals upstream of the overflow, geostrophically balanced flow at the sill, and a critical point near the sill (Dickson et al., 2008). A deepening of isopycnals was observed north of Denmark Strait (Girton et al., 2001), which is similar the result from this thesis (Section 3.2.5). Because a deepening happened north of Denmark Strait, they hypothesized that the hydraulic component of the overflow would decrease at Denmark Strait. Since sloping isopycnals were observed towards both Denmark Strait and the FBC (Figure 3.21c), this may be an indication of hydraulic control.

Hence, the main reason for the deepening of isopycnals towards the overflow regions is most likely to be hydraulic control at the sills. This forces the overflow layer to speed up due to a narrowing of the channel or change in thickness of the overflow layer. If the overflow layer becomes thicker or shallower, the velocity is impacted by this change. With corresponding structural changes in the Nordic Seas, the overflow layers may be thicker because of the decrease in density of the water masses supplied to the overflow. A thicker overflow layer will slow down the currents close to Denmark Strait or the FBC. The lighter GSAIW can more directly contribute to the overflow waters compared to the denser GSDW, which is observed from the decrease in density in the entire Nordic Seas and the changes in isopycnal depth.

Chapter 5

Conclusions

After the bottom convection ceased in the Greenland Sea in the 1980s, a warming trend started. The Greenland Sea became warmer and more saline. Around 10 years after the warming began in the Greenland Sea, the other basins also started to warm with increasing temperatures in the waters below 2000 m. The Greenland Sea is most likely the origin of the warming signal, because this is the area where the signal first was observed. The reduced convective activity in the Greenland Sea is most likely the main reason for the changes in hydrographic properties in the Nordic Seas. Increased temperature of the Atlantic Water inflow and the retreat of sea ice are both factors that have affected the strength of convection in the Greenland Sea.

The water masses in the Nordic Seas have over time become less dense. As the temperature and salinity started to increase from the 1980s, the density has been decreasing. From 1950–1979 to 2000–2018, the densities with the biggest proportion of the total volume have changed to lighter water masses. In the early period (1950–1979) densities around 28.08 – 28.09 kg/m^3 were most voluminous. From 2000 the density classes with the largest volume ranged from 28.05 to 28.07 kg/m^3. The main reason for this change can also be related to convective activity in the Greenland Sea. After 1994, the new and less dense GSAIW have been the main source of dense water from the Greenland Sea (Brakstad et al., 2019). The production of GSAIW resulted in a shoaling of the 28.05 kg/m^3 isopycnal in the Greenland Sea, while a deepening was found in the other basins. The main reason for this was the ceased supply of the denser GSDW.

The water masses in both the NIJ and IFSJ have become warmer, more saline and denser over the period 1950–2018 corresponding with the changes in the Greenland Sea. Estimation of Sigma-Pi distances show evidence that the densest source waters are likely formed in the Greenland Sea, in partic-

ular after 1994. The changing hydrographic properties in the Greenland Sea have affected the properties in the NIJ and IFSJ. It is important to maintain the density of the water masses in the NIJ and IFSJ. A less dense overflow will supply reduced volume of the densest water masses to the lower limb of the AMOC. This will then impact how the global circulation changes, because of the linked processes behind the changes.

Chapter 6

Future work

To get an even better understanding of the significant role the Greenland Sea has as the main source of dense water in the Nordic Seas, further work will be needed. This could be done by looking into how the convection and sea ice retreat have affected the density in the entire Nordic Seas, and then try to link the factors of the hydrographic and structural changes. Examining the change in sea ice concentration over the same time period can help to identify the beginning of the changes in the Greenland Sea. Then the next step will be to investigate how the sea ice retreat has impacted the entire Nordic Seas. The sea ice and convection in the gyres are well connected as the ice edge is the area with the highest heat loss and favours good conditions for convection.

Another topic that needs attention is the exchange of water masses between the Greenland Sea and its surroundings. Investigating the known areas of exchange from the Greenland Sea can help to identify the volume transport across the Mohn Ridge, through the Jan Mayen Channel, or the exchange between the Iceland and Greenland Seas. A better knowledge about the water mass exchange is important to identify the major pathways between the basins.

How the distribution of density classes has changed over the last 50 years is an important result. This topic needs a more specific focus and is of huge importance to understand the changes in the Nordic Seas. This can be done by comparing the densities of the dense water that are produced during winter in the Greenland Sea with the density classes that cover most of the total volume in the Nordic Seas. Comparing these two results might make it possible to trace the densest water masses back to the Greenland Sea.

To quantify the relative contribution from the Greenland Sea to overflows is also left to do. This can be done by comparing the amount of dense water

produced during winter in the Greenland Sea with the volume transported by the overflows. Since the hydrographic properties were changing in both the Greenland Sea and the overflow currents, a close connection between these two is likely to be found.

Bibliography

K. Aagaard and E. C. Carmack. The role of sea ice and other fresh water in the Arctic circulation. *Journal of Geophysical Research: Oceans*, 94(C10): 14485–14498, oct 1989. ISSN 0148-0227. doi: 10.1029/JC094iC10p14485. URL https://doi.org/10.1029/JC094iC10p14485.

G. Albertin. Piecewise linear least square fit, 2020. URL https://www.mathworks.com/matlabcentral/fileexchange/40913-piecewise-linear-least-square-fit.

A. Behrendt, H. Sumata, B. Rabe, and U. Schauer. A comprehensive, quality-controlled and up-to-date data set of temperature and salinity data for the Arctic Mediterranean Sea (Version 1.0), links to data files, 2017. URL https://doi.org/10.1594/PANGAEA.872931. Supplement to: Behrendt, A et al. (2017): UDASH - Unified Database for Arctic and Subarctic Hydrography. Earth System Science Data Discussions, 37 pp, https://doi.org/10.5194/essd-2017-92.

J. Blindheim and F. Rey. Water-mass formation and distribution in the Nordic Seas during the 1990s. *ICES Journal of Marine Science*, 61(5): 846–863, jan 2004. ISSN 1054-3139. doi: 10.1016/j.icesjms.2004.05.003. URL https://doi.org/10.1016/j.icesjms.2004.05.003.

A. Brakstad, K. Våge, L. Håvik, and G. W. K. Moore. Water Mass Transformation in the Greenland Sea during the Period 1986–2016. *Journal of Physical Oceanography*, 49(1):121–140, nov 2019. ISSN 0022-3670. doi: 10.1175/JPO-D-17-0273.1. URL https://doi.org/10.1175/JPO-D-17-0273.1.

A. Brakstad, G. Gebbie, V. K, and E. Jeansson. Tracing overflow water from the origin in the Nordic Seas to the Greenland-Scotland Ridge. in prep.

E. Carmack and K. Aagaard. On the deep water of the Greenland Sea. *Deep Sea Research and Oceanographic Abstracts*, 20(8):687–715, 1973. ISSN

0011-7471. doi: https://doi.org/10.1016/0011-7471(73)90086-7. URL http://www.sciencedirect.com/science/article/pii/0011747173900867.

B. Dickson, S. Dye, S. Jónsson, A. Köhl, A. Macrander, M. Marnela, J. Meincke, S. Olsen, B. Rudels, H. Valdimarsson, and G. Voet. *The Overflow Flux West of Iceland: Variability, Origins and Forcing*, pages 443–474. Springer Netherlands, Dordrecht, 2008. ISBN 978-1-4020-6774-7. doi: 10.1007/978-1-4020-6774-7_20. URL https://doi.org/10.1007/978-1-4020-6774-7_20.

R. R. Dickson and J. Brown. The production of North Atlantic Deep Water: Sources, rates, and pathways. *Journal of Geophysical Research: Oceans*, 99(C6):12319–12341, jun 1994. ISSN 0148-0227. doi: 10.1029/94JC00530. URL https://doi.org/10.1029/94JC00530.

J. Dugstad, I. Fer, J. LaCasce, M. Sanchez de La Lama, and M. Trodahl. Lateral Heat Transport in the Lofoten Basin: Near-Surface Pathways and Subsurface Exchange. *Journal of Geophysical Research: Oceans*, 124(5): 2992–3006, may 2019. ISSN 2169-9275. doi: 10.1029/2018JC014774. URL https://doi.org/10.1029/2018JC014774.

T. Eldevik, J. E. Ø. Nilsen, D. Iovino, K. Anders Olsson, A. B. Sandø, and H. Drange. Observed sources and variability of Nordic seas overflow. *Nature Geoscience*, 2(6):406–410, 2009. ISSN 1752-0908. doi: 10.1038/ngeo518. URL https://doi.org/10.1038/ngeo518.

J. B. Girton, T. B. Sanford, and R. H. Käse. Synoptic sections of the Denmark Strait Overflow. *Geophysical Research Letters*, 28(8):1619–1622, 2001. doi: 10.1029/2000GL011970. URL https://agupubs.onlinelibrary.wiley.com/doi/abs/10.1029/2000GL011970.

B. Hansen, S. Østerhus, W. R. Turrell, S. Jónsson, H. Valdimarsson, H. Hátún, and S. M. Olsen. *The Inflow of Atlantic Water, Heat, and Salt to the Nordic Seas Across the Greenland–Scotland Ridge*, pages 15–43. Springer Netherlands, Dordrecht, 2008. ISBN 978-1-4020-6774-7. doi: 10.1007/978-1-4020-6774-7_2. URL https://doi.org/10.1007/978-1-4020-6774-7_2.

B. Hansen, K. M. Húsgarð Larsen, H. Hátún, and S. Østerhus. A stable Faroe Bank Channel overflow 1995–2015. *Ocean Sci.*, 12(6):1205–1220, nov 2016. ISSN 1812-0792. doi: 10.5194/os-12-1205-2016. URL https:

//www.ocean-sci.net/12/1205/2016/https://www.ocean-sci.net/12/1205/2016/os-12-1205-2016.pdf.

B. E. Harden, R. S. Pickart, H. Valdimarsson, K. Våge, L. de Steur, C. Richards, F. Bahr, D. Torres, E. Børve, S. Jónsson, A. Macrander, S. Østerhus, L. Håvik, and T. Hattermann. Upstream sources of the Denmark Strait Overflow: Observations from a high-resolution mooring array. *Deep Sea Research Part I: Oceanographic Research Papers*, 112:94–112, 2016. ISSN 0967-0637. doi: https://doi.org/10.1016/j.dsr.2016.02.007. URL http://www.sciencedirect.com/science/article/pii/S0967063715301266.

J. Huang, R. S. Pickart, R. X. Huang, P. Lin, A. Brakstad, and F. Xu. Sources and upstream pathways of the densest overflow water in the Nordic Seas. *Nature Communications*, February 2020, in review.

R. X. Huang, L.-S. Yu, and S.-Q. Zhou. New Definition of Potential Spicity by the Least Square Method. *Journal of Geophysical Research: Oceans*, 123(10):7351–7365, oct 2018. ISSN 2169-9275. URL https://doi.org/10.1029/2018JC014306.

E. Jeansson, A. Olsen, and S. Jutterström. Arctic Intermediate Water in the Nordic Seas, 1991–2009. *Deep Sea Research Part I: Oceanographic Research Papers*, 128:82–97, 2017. ISSN 0967-0637. doi: https://doi.org/10.1016/j.dsr.2017.08.013. URL http://www.sciencedirect.com/science/article/pii/S0967063716300668.

K. Jochumsen, M. Moritz, N. Nunes, D. Quadfasel, K. M. H. Larsen, B. Hansen, H. Valdimarsson, and S. Jónsson. Revised transport estimates of the Denmark Strait overflow. *Journal of Geophysical Research: Oceans*, 122(4):3434–3450, apr 2017. ISSN 2169-9275. doi: 10.1002/2017JC012803. URL https://doi.org/10.1002/2017JC012803.

S. Jónsson. The circulation in the northern part of the Denmark Strait and its variability. *ICES CM*, 50:6, 1999. URL http://www.ices.dk/sites/pub/CMDoccuments/1999/L/L0699.pdf.

S. Jónsson and H. Valdimarsson. A new path for the Denmark Strait overflow water from the Iceland Sea to Denmark Strait. *Geophysical Research Letters*, 31(3), feb 2004. ISSN 0094-8276. doi: 10.1029/2003GL019214. URL https://doi.org/10.1029/2003GL019214.

S. Jónsson and H. Valdimarsson. Water mass transport variability to the North Icelandic shelf, 1994–2010. *ICES Journal of Marine Science*, 69(5):

809–815, feb 2012. ISSN 1054-3139. doi: 10.1093/icesjms/fss024. URL https://doi.org/10.1093/icesjms/fss024.

S. K. Lauvset, A. Brakstad, K. Våge, A. Olsen, E. Jeansson, and K. A. Mork. Continued warming, salinification and oxygenation of the Greenland Sea gyre. *Tellus, Series A: Dynamic Meteorology and Oceanography*, 70(1): 1–9, jan 2018. ISSN 16000870. doi: 10.1080/16000870.2018.1476434.

K. L. Lavender, W. Brechner Owens, and R. E. Davis. The mid-depth circulation of the subpolar North Atlantic Ocean as measured by subsurface floats. *Deep Sea Research Part I: Oceanographic Research Papers*, 52(5):767–785, 2005. ISSN 0967-0637. doi: https://doi.org/10.1016/j.dsr.2004.12.007. URL http://www.sciencedirect.com/science/article/pii/S0967063705000154.

A. Macrander, U. Send, H. Valdimarsson, S. Jónsson, and R. H Käse. Interannual changes in the overflow from the Nordic Seas into the Atlantic Ocean through Denmark Strait. *Geophysical Research Letters*, 32(6), 2005. ISSN 1944-8007. doi: 10.1029/2004GL021463.

S. A. Malmberg. Hydrographic investigations in the Iceland and Greenland Seas in late winter 1971-deep water project. *Jokull Reykjavik*, 1983.

J. Marshall and F. Schott. Open-ocean convection: Observations, theory, and models. *Reviews of Geophysics*, 37(1):1–64, 1999. doi: 10.1029/98RG02739. URL https://agupubs.onlinelibrary.wiley.com/doi/abs/10.1029/98RG02739.

D. Mastropole, R. S. Pickart, H. Valdimarsson, K. Våge, K. Jochumsen, and J. Girton. On the hydrography of Denmark Strait. *Journal of Geophysical Research: Oceans*, 122(1):306–321, jan 2017. ISSN 2169-9275. doi: 10.1002/2016JC012007. URL https://doi.org/10.1002/2016JC012007.

T. J. McDougall and P. M. Barker. Getting started with TEOS-10 and the Gibbs Seawater (GSW) oceanographic toolbox. *SCOR/IAPSO WG*, 127: 1–28, 2011.

J. Meincke, S. Jónsson, and J. H. Swift. *Variability of convective conditions in the Greenland Sea*, volume 195. 1992.

J. Meincke, B. Rudels, and H. J. Friedrich. The Arctic Ocean–Nordic Seas thermohaline system. *ICES Journal of Marine Science*, 54(3):283–299, jun 1997. ISSN 1054-3139. doi: 10.1006/jmsc.1997.0229. URL https://doi.org/10.1006/jmsc.1997.0229.

G. W. K. Moore, K. Våge, R. S. Pickart, and I. A. Renfrew. Decreasing intensity of open-ocean convection in the Greenland and Iceland seas. *Nature Climate Change*, 5:877, jun 2015. URL https://doi.org/10.1038/nclimate2688http://10.0.4.14/nclimate2688https://www.nature.com/articles/nclimate2688{\#}supplementary-information.

K. A. Mork, K. F. Drinkwater, S. Jónsson, H. Valdimarsson, and M. Ostrowski. Water mass exchanges between the Norwegian and Iceland seas over the Jan Mayen Ridge using in-situ current measurements. *Journal of Marine Systems*, 139:227–240, 2014. ISSN 0924-7963. doi: https://doi.org/10.1016/j.jmarsys.2014.06.008. URL http://www.sciencedirect.com/science/article/pii/S0924796314001596.

K. A. Mork, Ø. Skagseth, and H. Søiland. Recent Warming and Freshening of the Norwegian Sea Observed by Argo Data. *Journal of Climate*, 32(12): 3695–3705, mar 2019. ISSN 0894-8755. doi: 10.1175/JCLI-D-18-0591.1. URL https://doi.org/10.1175/JCLI-D-18-0591.1.

W. H. Munk. Chapter 9, internal waves and small-scale processes. *Evolution of Physical Oceanography*, pages 264–291, 1981. URL https://ci.nii.ac.jp/naid/10025033094/en/.

J. Nilsen, H. Hatun, K. Mork, and H. Valdimarsson. The NISE dataset. *Technical Report0807. Trshavn, Faroe Islands*, 117, 2008.

O. A. Nøst and P. E. Isachsen. The large-scale time-mean ocean circulation in the Nordic Seas and Arctic Ocean estimated from simplified dynamics. *Journal of Marine Research*, 61(2):175–210, 2003. ISSN 0022-2402. doi: doi:10.1357/002224003322005069. URL https://www.ingentaconnect.com/content/jmr/jmr/2003/00000061/00000002/art00002.

S. Østerhus and T. Gammelsrød. The abyss of the Nordic Seas is warming. *Journal of Climate*, 12(11):3297–3304, nov 1999. ISSN 0894-8755. doi: 10.1175/1520-0442(1999)012<3297:TAOTNS>2.0.CO;2. URL https://doi.org/10.1175/1520-0442(1999)012{\%}3C3297:TAOTNS{\%}3E2.0.COhttp://0.0.0.2.

J. Palsson, O. S. Astthorsson, and H. Valdimarsson. Hydrographic variability in Icelandic waters during recent decades and related changes in distribution of some fish species. *ICES Journal of Marine Science*, 69(5): 816–825, mar 2012. ISSN 1054-3139. doi: 10.1093/icesjms/fss027. URL https://dx.doi.org/10.1093/icesjms/fss027.

R. S. Pickart and W. M. Smethie. Temporal evolution of the deep western boundary current where it enters the sub-tropical domain. *Deep Sea Research Part I: Oceanographic Research Papers*, 45(7):1053–1083, 1998. ISSN 0967-0637. doi: https://doi.org/10.1016/S0967-0637(97)00084-8. URL http://www.sciencedirect.com/science/article/pii/S0967063797000848.

R. S. Pickart, M. A. Spall, D. J. Torres, K. Våge, H. Valdimarsson, C. Nobre, G. W. K. Moore, S. Jónsson, and D. Mastropole. The North Icelandic Jet and its relationship to the North Icelandic Irminger Current. *Journal of Marine Research*, 75:605–639, 2017. URL https://doi.org/10.1357/002224017822109505.

S. Semper, K. Våge, R. S. Pickart, H. Valdimarsson, D. J. Torres, and S. Jónsson. The emergence of the North Icelandic Jet and its evolution from northeast Iceland to Denmark Strait. *Journal of Physical Oceanography*, jul 2019. ISSN 0022-3670. doi: 10.1175/JPO-D-19-0088.1. URL https://doi.org/10.1175/JPO-D-19-0088.1.

S. Semper, R. Pickart, K. Våge, K. Larsen, H. Hátún, and B. Hansen. The Iceland-Faroe Slope Jet: A conduit for dense water toward the Faroe Bank Channel overflow. *Nature Communications*, in review.

Q. Shao, J. Zhao, K. F. Drinkwater, X. Wang, and Y. Cao. Internal overflow in the Nordic Seas and the cold reservoir in the northern Norwegian Basin. *Deep Sea Research Part I: Oceanographic Research Papers*, apr 2019. ISSN 0967-0637. doi: 10.1016/J.DSR.2019.04.012. URL https://www.sciencedirect.com/science/article/pii/S0967063718302619?via{\%}3Dihub.

Ø. Skagseth and K. A. Mork. Heat content in the Norwegian Sea, 1995–2010. *ICES Journal of Marine Science*, 69(5):826–832, jul 2012. ISSN 1054-3139. URL http://dx.doi.org/10.1093/icesjms/fss026.

R. Somavilla. Draining and Upwelling of Greenland Sea Deep Waters. *Journal of Geophysical Research: Oceans*, 124(4):2842–2860, apr 2019. ISSN 2169-9275. doi: 10.1029/2018JC014249. URL https://doi.org/10.1029/2018JC014249.

M. A. Spall. Non-local topographic influences on deep convection: An idealized model for the Nordic Seas. *Ocean Modelling*, 32(1):72 – 85, 2010. ISSN 1463-5003. doi: https://doi.org/10.1016/j.ocemod.2009.10.009. URL

http://www.sciencedirect.com/science/article/pii/S1463500309002054.

R. E. Thomson and W. J. Emery. Chapter 3 - statistical methods and error handling. In R. E. Thomson and W. J. Emery, editors, *Data Analysis Methods in Physical Oceanography (Third Edition)*, pages 219 – 311. Elsevier, Boston, third edition edition, 2014. ISBN 978-0-12-387782-6. doi: https://doi.org/10.1016/B978-0-12-387782-6.00003-X. URL http://www.sciencedirect.com/science/article/pii/B978012387782600003X.

R. E. Todd, D. L. Rudnick, M. R. Mazloff, B. D. Cornuelle, and R. E. Davis. Thermohaline structure in the california current system: Observations and modeling of spice variance. *Journal of Geophysical Research: Oceans*, 117 (C2), 2012. doi: 10.1029/2011JC007589. URL https://agupubs.onlinelibrary.wiley.com/doi/abs/10.1029/2011JC007589.

K. Våge, R. S. Pickart, M. A. Spall, H. Valdimarsson, S. Jónsson, D. J. Torres, S. Østerhus, and T. Eldevik. Significant role of the North Icelandic Jet in the formation of Denmark Strait overflow water. *Nature Geoscience*, 4:723, aug 2011. URL https://doi.org/10.1038/ngeo1234http://10.0.4.14/ngeo1234https://www.nature.com/articles/ngeo1234{\#}supplementary-information.

K. Våge, R. S. Pickart, M. A. Spall, G. W. K. Moore, H. Valdimarsson, D. J. Torres, S. Y. Erofeeva, and J. E. Ø. Nilsen. Revised circulation scheme north of the Denmark Strait. *Deep Sea Research Part I: Oceanographic Research Papers*, 79:20–39, 2013. ISSN 0967-0637. doi: https://doi.org/10.1016/j.dsr.2013.05.007. URL http://www.sciencedirect.com/science/article/pii/S0967063713001040.

K. Våge, G. W. K. Moore, S. Jónsson, and H. Valdimarsson. Water mass transformation in the Iceland Sea. *Deep Sea Research Part I: Oceanographic Research Papers*, 101:98–109, 2015. ISSN 0967-0637. doi: https://doi.org/10.1016/j.dsr.2015.04.001. URL http://www.sciencedirect.com/science/article/pii/S0967063715000680.

G. Voet, D. Quadfasel, K. A. Mork, and H. Søiland. The mid-depth circulation of the Nordic Seas derived from profiling float observations. *Tellus A: Dynamic Meteorology and Oceanography*, 62(4):516–529, jan 2010. ISSN null. doi: 10.1111/j.1600-0870.2009.00444.x. URL https://www.tandfonline.com/doi/abs/10.1111/j.1600-0870.2009.00444.x.

X. Wang, J. Zhao, T. Li, W. Zhong, and Y. Jiao. Deep waters warming in the Nordic Seas from 1972 to 2013. *Acta Oceanologica Sinica*, 34(3): 18–24, 2015. ISSN 1869-1099. doi: 10.1007/s13131-015-0613-z. URL https://doi.org/10.1007/s13131-015-0613-z.